NEUROSCIENCE

GPR39 regulated spinal glycinergic inhibition and mechanical inflammatory pain

Hu-Hu Bai[1,2], Kang-Li Wang[1], Xiang-Ru Zeng[1], Jing Li[1], Yuan Li[1], Jia-Yu Xu[1], Yue Zhang[3], Hai-Feng Jiang[3], Xian Yang[1], Zhan-Wei Suo[1], Xiao-Dong Hu[1]*

G protein–coupled receptor 39 (GPR39) senses the change of extracellular divalent zinc ion and signals through multiple G proteins to a broad spectrum of downstream effectors. Here, we found that GPR39 was prevalent at inhibitory synapses of spinal cord somatostatin-positive (SOM^+) interneurons, a mechanosensitive subpopulation that is critical for the conveyance of mechanical pain. GPR39 complexed specifically with inhibitory glycine receptors (GlyRs) and helped maintain glycinergic transmission in a manner independent of G protein signalings. Targeted knockdown of GPR39 in SOM^+ interneurons reduced the glycinergic inhibition and facilitated the excitatory output from SOM^+ interneurons to spinoparabrachial neurons that engaged superspinal neural circuits encoding both the sensory discriminative and affective motivational domains of pain experience. Our data showed that pharmacological activation of GPR39 or augmenting GPR39 interaction with GlyRs at the spinal level effectively alleviated the sensory and affective pain induced by complete Freund's adjuvant and implicated GPR39 as a promising therapeutic target for the treatment of inflammatory mechanical pain.

INTRODUCTION

Mechanical pain induced by tissue or nerve injury typically manifests as an increased sensitivity to innocuous mechanical stimuli or movement. The dorsal horn of spinal cord serves as a key site that receives, integrates, and transmits the mechanosensory information (*1*–*3*). The gate control theory of pain predicts that the primary afferent low-threshold mechanoreceptors (LTMRs) send direct projection onto spinal mechanosensitive interneurons, through which the innocuous input is anatomically linked to ascending pain pathways (*2*, *4*, *5*). This pre-existing neural circuit is silent under physiological conditions due to the strong feedforward activation by LTMRs of local GABAergic and/or glycinergic inhibitory interneurons (*1*, *6*, *7*). Following tissue or nerve injury, the spinal inhibition is reduced, which permits the excitatory output from mechanosensory interneurons to projection neurons (*1*, *8*). The somatostatin-positive (SOM^+) excitatory neurons represent a subset of mechanosensory interneurons important for the conveyance of mechanosensory information to spinal projection neurons (*9*–*11*). The projection neurons send afferents to thalamic nuclei for sensory discrimination and to a variety of brainstem and telencephalic nuclei for processing the affective component associated with body injury (*12*–*15*). The genetic ablation of spinal SOM^+ neurons blocks the mechanical allodynia in both inflammatory and neuropathic pain conditions (*10*, *11*). Although much progress has been made in our understanding of the cellular and circuit mechanisms for sensory mechanotransduction, the effective and safe treatment of chronic pain remains a clinical challenge. For example, the current treatments for inflammatory pain are largely limited by side effects, such as the cardiovascular effects associated with the long-term use of cyclooxygenase inhibitors.

Divalent zinc ion (Zn^{2+}) is a well-established anti-inflammatory agent that has long been known for pain relief (*16*, *17*). In the nervous system, Zn^{2+} is an important neuromodulator that is stored in the synaptic vesicles of both excitatory and inhibitory neurons (*18*–*21*). When coreleased with neurotransmitters into synaptic clefts, Zn^{2+} binds to several ionotropic receptors, such as excitatory *N*-methyl-D-aspartate (NMDA) subtype glutamate receptors (NMDARs) and inhibitory glycine receptors (GlyRs) (*22*). Synaptic Zn^{2+} also triggers metabotropic signalings, a process that is ascribed to the activation of G protein–coupled receptor 39 (GPR39) (*23*). The Zn^{2+}-sensitive GPR39 belongs to the ghrelin/neurotensin receptor family with a high degree of constitutive activities toward $G\alpha_{q/11}$, $G\alpha_{12/13}$, and Gαs proteins (*24*, *25*). Promiscuous couplings to multiple G proteins enable GPR39 to integrate complex signaling networks that shape synaptic strength and neuronal excitability. The widely distributed GPR39 has been implicated in several psychiatric disorders (*26*). Here, we found a specific interaction of GPR39 with inhibitory GlyRs and revealed a G protein–independent mechanism by which GPR39 modulated the feedforward glycinergic input onto spinal SOM^+ interneurons. Our data showed that GPR39 gated the relay of mechanosensory information from SOM^+ interneurons to spinoparabrachial neurons (SPNs) and provided evidence that GPR39 might serve as a promising target for the alleviation of mechanical pain.

RESULTS

Mechanical pain evoked by GPR39 knockdown in spinal SOM^+ interneurons

To investigate the role of GPR39 in pain perception, we first conducted behavioral assessments in global *GPR39* knockout ($GPR39^{-/-}$) mice. There was no difference in the heat or cold nociceptive sensitivity between $GPR39^{-/-}$ and wild-type (WT) mice (fig. S1, A and B). The von Frey test showed, however, that the thresholds for reflexive withdrawals were significantly lower in $GPR39^{-/-}$ mice relative to WT ones (fig. S1C), indicating the hypersensitivity to punctate mechanical force in the absence of GPR39. To test whether GPR39 knockout evoked dynamic mechanical allodynia, we used a custom-made soft paintbrush to stroke the plantar surfaces of hindpaws (*11*). Compared to WT controls, $GPR39^{-/-}$ mice displayed pronounced licking and guarding behaviors in response to brush stimulation (fig. S1D).

[1]Department of Molecular Pharmacology, School of Pharmacy, Lanzhou University, Lanzhou, Gansu 730000, P.R. China. [2]School of Life Science, Lanzhou University, Lanzhou, Gansu 730000, P.R. China. [3]School of Public Health, Gansu University of Chinese medicine, Lanzhou, Gansu 730000, P.R. China.
*Corresponding author. Email: huxxiaodong@lzu.edu.cn

The dorsal horn of spinal cord is a key site for the integration and transmission of mechanoreceptive signals. To characterize the laminar distribution of GPR39 in the spinal cord of adult mice, we outlined the ventral inner layer of lamina II by labeling protein kinase Cγ-positive (PKCγ$^+$) interneurons. The outer and dorsal inner layers of lamina II were marked by the central terminals of primary sensory neurons positive for calcitonin gene–related peptide (CGRP$^+$) and isolectin B4 (IB4$^+$), respectively (*10*). Most of the GPR39-positive cells were localized dorsal to PKCγ$^+$ interneurons and were intertwined with CGRP$^+$ and IB4$^+$ terminals (Fig. 1A). Previous studies have detected GPR39 in the microglial cells in human and rat brains, which modulates neuroinflammation (*27*, *28*). In the spinal cords of mice, GPR39 was not coincident with astrocyte marker glial fibrillary acidic protein (GFAP) or microglia marker OX-42 (Fig. 1B). We found that the expression of GPR39 was confined to neuronal nuclei-positive (NeuN$^+$) superficial dorsal horn neurons (Fig. 1C). To validate the specificity of GPR39 antibody, we performed immunohistochemistry in *GPR39*$^{-/-}$ mice, finding that GPR39 knockout completely diminished the GPR39 immunoreactive signals (Fig. 1C).

The spinal cord neuronal circuits transmitting mechanical pain involve several mechanosensitive neuron subtypes, of which somatostatin-positive (SOM$^+$) excitatory interneurons are located dorsal to PKCγ$^+$ neurons and are critical for both dynamic and static allodynia (*10*, *11*). Given that GPR39 deletion elicited the mechanical pain, we tested whether GPR39 was expressed in SOM$^+$ interneurons. We labeled SOM$^+$ neurons with tdTomato by crossing SOM-Cre mice with Ai9 reporter mice (referred to as SOM-tdTomato mice). Immunofluorescence showed that 77% of SOM$^+$ neurons expressed GPR39 (Fig. 1D), and 41% of GPR39$^+$ neurons were positive for tdTomato ($n = 11$ sections from three mice).

To test if GPR39 expressed in spinal SOM$^+$ interneurons was required for pain modification, we targeted a Cre-inducible adeno-associated virus (AAV) carrying short hair RNA (shRNA) against GPR39 (AAV2/9-EF1α-DIO-shRNA-GPR39-EGFP) into the L4-L5 lumbar spinal cord segments of SOM-tdTomato mice to knock down GPR39 (fig. S2A). The viral expression was restricted to the spinal cord and was excluded from dorsal root ganglia (DRG) (fig. S2B). The freely moving mice with specific GPR39 knockdown in SOM$^+$ interneurons exhibited a marked increase in spontaneous licking behavior (Fig. 1E). No change of the locomotor activity was seen after shRNA-GPR39 expression, as evidenced by the comparable total traveling distance (Fig. 1F) and mean velocity (Fig. 1G) to enhanced green fluorescent protein (EGFP) control mice. The von Frey test showed that shRNA-GPR39 caused a notable reduction of the reflexive withdrawal thresholds in comparison to EGFP control (Fig. 1H). Increasingly punctate forces also evoked attending (paw guarding and licking) and escape behaviors (Fig. 1I). These pain behaviors were more prominent in GPR39 knockdown mice than EGFP controls (Fig. 1I). We then measured the dynamic allodynia and found the hypersensitivity of GPR39 knockdown mice to the gentle stroking of the plantar surfaces of hindpaws with a paintbrush (Fig. 1J). To test whether a negative valence was assigned to the light touch when spinal SOM$^+$ interneurons were deficient in GPR39, we performed a conditioned place aversion (CPA) assay. The mice expressing shRNA-GPR39, but not EGFP control, displayed avoidance of the chamber where they received inescapable brush stroking (Fig. 1K), suggesting that selective GPR39 knockdown in SOM$^+$ interneurons enabled the light touch to recruit supraspinal circuits for aversive pain memory. In the Hargreaves and acetone evaporative cooling tests, we did not detect notable changes in the heat and cold sensitivities after GPR39 knockdown (fig. S3), supporting the modality specificity of SOM$^+$ interneurons in the processing of sensory inputs.

Role of GPR39 in feedforward glycinergic inhibition of SOM$^+$ interneurons

To investigate how GPR39 modulated pain transmission, we recorded the miniature excitatory postsynaptic currents mediated by AMPA receptors (AMPAR-mEPSCs) on SOM$^+$ interneurons at day 21 after intraspinal injection of AAV2/9-EF1α-DIO-shRNA-GPR39-EGFP in SOM-Cre mice. The results showed that GPR39 knockdown did not affect the amplitudes and frequencies of AMPAR-mEPSCs when compared to EGFP control (fig. S4A). The dorsal root–evoked EPSCs (eEPSCs) mediated by NMDA receptors (NMDAR-eEPSCs) were also comparable between neurons expressing EGFP and shRNA-GPR39 (fig. S4B). We then recorded the miniature inhibitory postsynaptic currents mediated by γ-aminobutyric acid type A ($GABA_A$) receptors ($GABA_A$R-mIPSCs). Again, no difference was found in GABAergic synaptic responses between EGFP and shRNA-GPR39 neurons (fig. S4C). GlyR is another inhibitory receptor that gates mechanical pain transmission (*1*). Our data showed that GPR39 knockdown significantly reduced the amplitudes of GlyR-mIPSCs (Fig. 2A), while the frequencies of GlyR-mIPSCs, a readout of presynaptic release probability, were unaltered (Fig. 2A). These results implied that inhibitory GlyRs were the specific target for GPR39 regulation. To examine whether GPR39 was present at inhibitory synapses, we labeled SOM$^+$ interneurons by injecting AAV2/9-EF1α-DIO-EGFP into the lumbar spinal cords of SOM-Cre mice and performed double immunofluorescence for GPR39 and inhibitory postsynaptic marker gephyrin (Fig. 2B). The GPR39 immunoreactivity was detected in 57% of gephyrin$^+$ synapses ($n = 5$ sections from two mice), and 67% of GPR39$^+$ puncta were coincident with gephyrin immunosignals (Fig. 2B).

To test if the loss of glycinergic inhibition after GPR39 ablation caused the hyperexcitability of SOM$^+$ neurons, we elicited the action potentials (APs) by depolarizing current injections under the whole-cell current-clamp configuration. The neurons we recorded exhibited either the delayed- or bursting-firing pattern at the holding membrane potential of −60 mV (Fig. 2C) (*10*, *29*). Compared to EGFP control, GPR39 knockdown led to a notable increase in the AP firing frequencies of SOM$^+$ interneurons (Fig. 2C). Meanwhile, GPR39 knockdown reduced the rheobase (Fig. 2D), increased the membrane resistance (Fig. 2E), and shifted the resting membrane potential to be more positive (Fig. 2F), suggesting that GPR39 was tonically active in the negative control of SOM$^+$ neuron excitability.

The low-threshold β-amyloid (Aβ) fiber input has been shown to elicit the excitation and feedforward inhibition of SOM$^+$ interneurons (Fig. 2G) (*10*, *11*). Disinhibition in the context of chronic pain conditions is proposed as a key mechanism by which Aβ afferents drive the excitatory output from SOM$^+$ interneurons to spinal cord nociceptive circuits leading to mechanical allodynia (*10*, *11*). Given the necessity of GPR39 for normal glycinergic transmission, we sought to examine the responses of SOM$^+$ neurons to Aβ fiber input in the absence of GPR39. The electrical stimulation of dorsal roots at Aβ fiber strength (25 μA) evoked the excitatory postsynaptic potentials in EGFP-expressing control

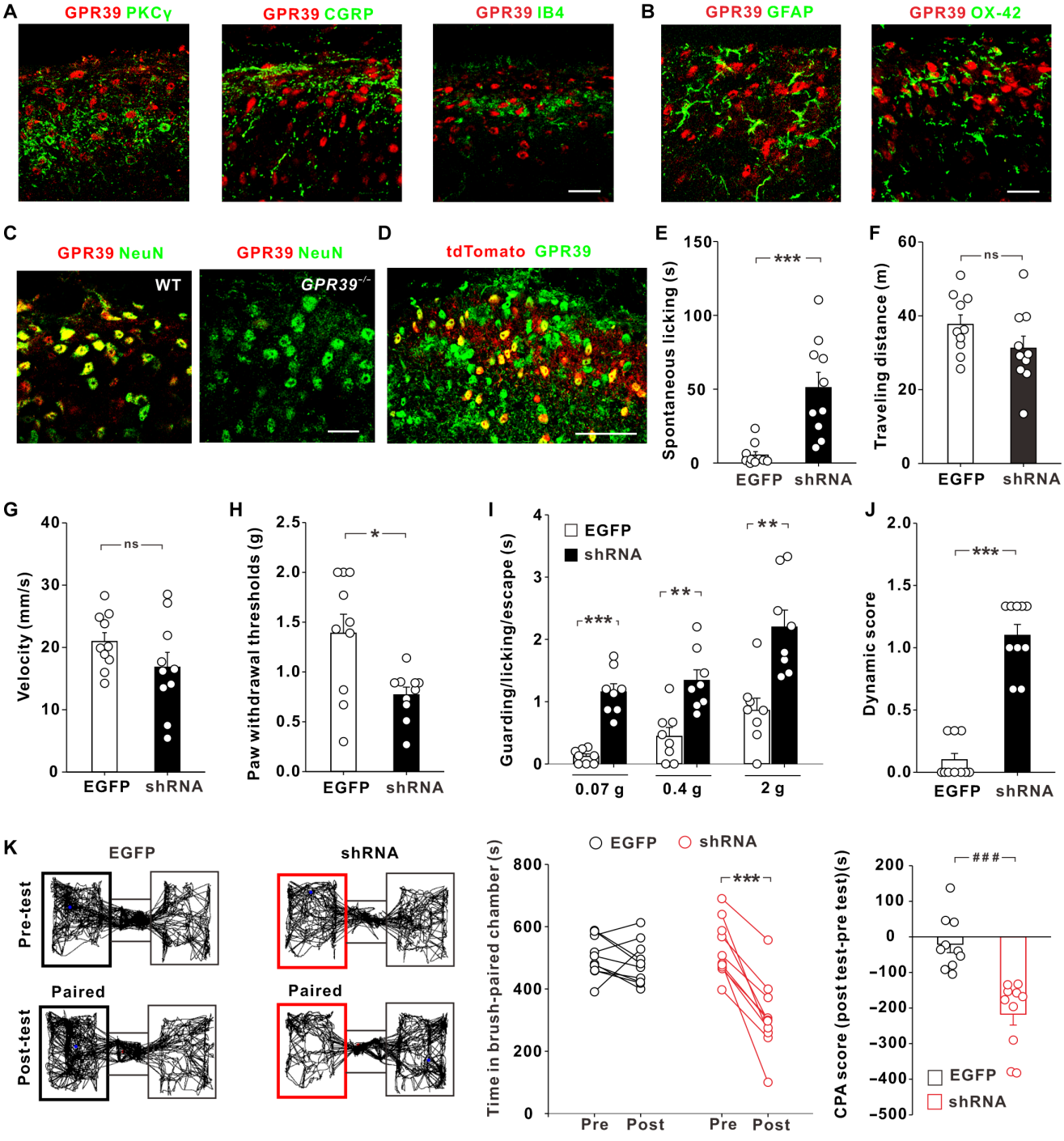

Fig. 1. GPR39 knockdown in spinal cord SOM$^+$ interneurons evoked mechanical pain in mice. (**A**) Double immunofluorescence for GPR39 (red) and PKCγ, CGRP, or IB4 (green) in spinal sections. Scale bar,20 μm. (**B**) Immunofluorescence for GPR39 (red) and astrocyte marker GFAP or microglia marker OX-42 (green). Scale bar, 20 μm. (**C**) Immunostaining of GPR39 (red) and NeuN (green) in spinal sections from WT and *GPR39*$^{-/-}$ mice. Scale bar, 20 μm. (**D**) Spinal sections from SOM-tdTomato mice showing tdTomato (red) and GPR39 signals (green). Scale bar, 50 μm. (**E**) Spontaneous licking activities of mice with spinal SOM$^+$ interneurons transfected with AAV2/9-EF1α-DIO-EGFP [enhanced green fluorescent protein (EGFP)] or AAV2/9-EF1α-DIO-shRNA-GPR39-EGFP (shRNA). ***$P < 0.001$ (Mann-Whitney *U* test, $n = 10$ mice per group). (**F** and **G**) Traveling distance [F; ns (not significant), $P = 0.113$, Mann-Whitney *U* test] and mean velocity (G; ns, $P = 0.387$, Mann-Whitney *U* test) of mice with spinal SOM$^+$ interneurons expressing EGFP or shRNA ($n = 10$ mice per group). (**H** and **I**) Reflexive withdrawal thresholds (H; *$P = 0.035$, Mann-Whitney *U* test, $n = 10$ mice per group) and attending/escape behaviors to von Frey filament stimuli (I; **$P = 0.002$ and ***$P < 0.001$, Mann-Whitney *U* test, $n = 8$ mice per group). (**J**) Brush-evoked pain responses. ***$P < 0.001$ (Mann-Whitney *U* test; $n = 10$ mice per group). (**K**) Brushing evoked conditioned place aversion (CPA) in mice with spinal SOM$^+$ neurons expressing shRNA but not EGFP control ($n = 10$ mice per group). ***$P < 0.001$ ($t_9 = 7.085$, paired Student's *t* test) and ###$P < 0.001$ (Mann-Whitney *U* test).

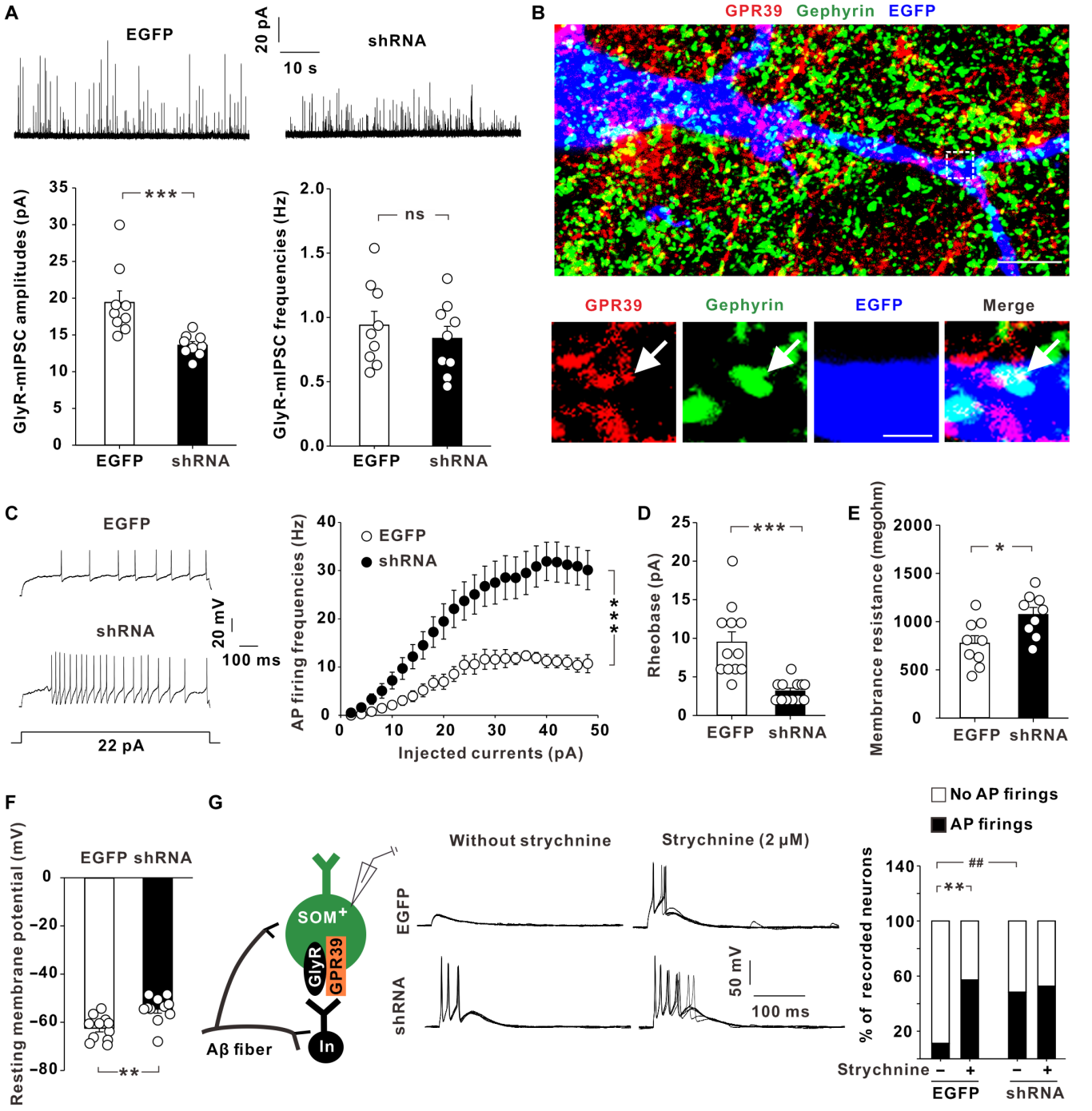

Fig. 2. GPR39 was integral to normal glycinergic input onto SOM$^+$ interneurons. (**A**) GlyR-mIPSCs recorded on SOM$^+$ interneurons at day 21 after intraspinal injection of AAV2/9-EF1α-DIO-EGFP (EGFP) or AAV2/9-EF1α-DIO-shRNA-GPR39-EGFP (shRNA) in SOM-Cre mice. ***$P < 0.001$ and ns, $P = 0.605$ (Mann-Whitney U test). $n = 9$ neurons from six mice per group. (**B**) Immunofluorescence for GPR39 and gephyrin at day 21 after intraspinal injection of AAV2/9-EF1α-DIO-EGFP in SOM-Cre mice. The boxed area (top) was shown with higher magnification (bottom). The arrow indicated the colocalization. Scale bars, 5 μm (top) and 2 μm (bottom). (**C**) Current-clamp recordings of AP firings elicited by depolarizing current injections in SOM$^+$ interneurons expressing EGFP or shRNA (left). The firing frequencies at all current injection levels were quantified (right). $F_{23,874} = 6.909$, ***$P < 0.001$ (repeated measurement). $n = 20$ neurons from 10 mice per group. (**D** to **F**) Rheobase (D, ***$P < 0.001$, Mann-Whitney U test, $n = 12$ neurons per group), membrane resistance (E, *$P = 0.014$, Mann-Whitney U test, $n = 9$ neurons per group), and resting membrane potential (F; **$P = 0.002$, Mann-Whitney U test, $n = 11$ neurons per group) of SOM$^+$ interneurons expressing EGFP or shRNA. (**G**) Current-clamp recordings of AP firings evoked by electrical stimulation of dorsal roots at β-amyloid (Aβ) fiber intensity (25 μA) on SOM$^+$ neurons expressing EGFP or shRNA before and after strychnine (2 μM) perfusion. **$P = 0.003$ ($\chi 2 = 8.925$) and ##$P = 0.009$ ($\chi 2 = 6.832$), Pearson's chi-square test. In, inhibitory neurons.

neurons at resting membrane potentials (*10*, *11*). However, only 11.1% (2 of 18) of the recorded control SOM$^+$ interneurons fired APs in response to Aβ fiber activation (Fig. 2G). When glycinergic inhibition was removed by bath perfusion of GlyR-selective antagonist strychnine (2 μM), the Aβ fiber stimulation evoked AP discharge in 57.1% (12/21) of EGFP neurons (Fig. 2G), suggesting a critical role of feedforward glycinergic inhibitory input in the control of AP output from SOM$^+$ neurons. Next, we knocked down GPR39 in SOM$^+$ neurons. In this case, 48.3% (14 of 29) of the recorded neurons responded to Aβ fiber stimulation with AP firings (Fig. 2G), a proportion significantly higher than that observed in EGFP control neurons (Fig. 2G). With GPR39 knockdown, bath strychnine application failed to cause a further increase in the percentage (52.6%; 10 of 19) of neurons with AP output (Fig. 2G). These results indicated an important role of GPR39 in the gating of touch-sensitive Aβ fiber input to SOM$^+$ interneurons that relay mechanical allodynia.

Inhibition by GPR39 of glutamatergic output from SOM$^+$ interneurons to spinoparabrachial projection neurons

The activation of SOM$^+$ interneurons has been implicated in the recruitment of SPNs, a spinal neural circuit that engages the brain regions encoding the affective dimension of pain experience (*9*, *13*, *14*). To test if SOM$^+$ interneurons directly synapsed onto SPNs, we injected a Cre-dependent viral construct AAV2/9-EF1α-DIO-ChR2(H134R)-mCherry to the dorsal horn of SOM-Cre mice and performed the whole-cell voltage-clamp recordings on the lamina I SPNs that were labeled through the injection of retrograde tracer cholera toxin subunit-B 488 (CTB-488) into the lateral parabrachial nuclei (Fig. 3A). Photoactivation of SOM$^+$ neuron axon terminals eEPSCs in the SPNs (Fig. 3B). In 5 of the 11 recorded neurons, the synaptic currents were blocked by bath application of tetrodotoxin (TTX; 1 μM) and rescued by superimposing 4-aminopyridine (100 μM; Fig. 3B), suggesting a monosynaptic contact between SOM$^+$ neurons and SPNs. In six of the recorded SPNs, the light-eEPSCs were eliminated by TTX but could not be rescued by 4-aminopyridine (Fig. 3C), indicating a polysynaptic transmission from SOM$^+$ interneurons to SPNs.

To investigate whether GPR39 influenced the excitatory output from SOM$^+$ interneurons to SPNs, we virally expressed shRNA-GPR39 in SOM$^+$ interneurons and recorded spontaneous EPSCs (sEPSCs) on lamina I SPNs. Compared to EGFP control, specific GPR39 knockdown in SOM$^+$ interneurons increased the frequencies of sEPSCs with the sEPSC amplitudes unaltered (Fig. 3D), suggesting that SOM$^+$ interneurons became an important source of excitatory input onto SPNs once GPR39 was deleted. We then recorded spontaneous firings of SPNs at resting membrane potentials (Fig. 3E). Compared to EGFP control, selective GPR39 knockdown in SOM$^+$ interneurons enabled SPNs to generate spontaneous AP output in a higher rate (Fig. 3E). In agreement with these results, GPR39 deletion in SOM$^+$ interneurons increased the expression of c-fos, a proxy for neuron activation, in SPNs that were labeled by injecting retrograde tracer CTB-555 into the lateral parabrachial nuclei (Fig. 3F). Meanwhile, the number of c-fos$^+$ neurons in the lateral parabrachial nuclei was also higher after GPR39 knockdown in spinal SOM$^+$ interneurons when compared to EGFP control (Fig. 3G). These data suggested that GPR39 negatively controlled the synaptic transmission from SOM$^+$ interneurons to ascending supraspinal pain pathways.

Direct interaction between GPR39 and GlyR

The specificity of GPR39 in regulating GlyR currents prompted us to test if there was a direct interaction between these two proteins. To this end, the proximity ligation assay (PLA) was performed in EGFP-labeled SOM$^+$ interneurons in slices from L4-L5 spinal segments. The PLA detection of GPR39–GlyR α1 proximity produced dense punctate signals in SOM$^+$ interneurons (Fig. 4A), and these PLA signals were invisible if GlyR α1 antibody was omitted (fig. S5A), suggesting that endogenous GPR39 complexed with GlyR α1 under normal conditions. The complex formation between GPR39 and GlyR α1 required the presence of extracellular Zn^{2+} because a cell-impermeable Zn^{2+} chelator Ca-EDTA (25 nmol), when spinally given before PLA detection, significantly reduced the punctate signals (Fig. 4A). To further investigate the dynamics of GPR39–GlyR α1 complex under pathological pain condition, we injected complete Freund's adjuvant (CFA) into the plantar surfaces of hindpaws to model the inflammatory pain. Compared to saline control, CFA injection decreased the PLA signals in spinal SOM$^+$ interneurons (Fig. 4B). Intrathecal application of exogenous Zn^{2+} (20 nmol) resumed the PLA signals in inflamed mice, consolidating the role of Zn^{2+} in GPR39–GlyR α1 complex formation (Fig. 4B). Because Zn^{2+} simultaneously modulates GlyR α1 activity (*30*, *31*), we next selected a GPR39-specific agonist TC-G 1008 (*N*-[3-chloro-4-[[[2-(methylamino)-6-(2-pyridinyl)-4-pyrimidinyl] amino] methyl]phenyl]methanesulfonamide) (*32*, *33*). Spinal treatment with TC-G 1008 (50 pmol) led to a similar rescue of the PLA puncta as with Zn^{2+} (Fig. 4B). Peripheral inflammation or spinal Zn^{2+} and TC-G 1008 application did not affect the total protein levels of GPR39 and GlyR α1 (fig. S6), excluding the possibility that the altered protein expression affected the PLA signal dynamics.

To confirm the direct interaction of GPR39 with GlyR α1, we conducted glutathione *S*-transferase (GST) pull-down assay in vitro. The intracellular large loop (ILL) of GlyR α1 (GlyR α1–ILL), a structural motif critical for the recruitment of intracellular signaling components (*34*), pulled down Flag-tagged GPR39 (Flag-GPR39) from the lysates of transfected human embryonic kidney (HEK) 293T cells (Fig. 4C). By comparison, the corresponding loop of GlyR α3 subunit (GlyR α3–ILL), another GlyR isoform involved in pain modification (*35*), failed to precipitate Flag-GPR39 (Fig. 4C). The ILL of GlyR β subunit (GlyR β–ILL), which is important for the synaptic trafficking of GlyRs (*36*–*38*), also failed to pull down Flag-GPR39 (Fig. 4D). With regard to the GPR39 region responsible for GlyR α1 binding, we identified the extreme carboxyl tail of GPR39 (GPR39ct) that immunoprecipitated GlyR α1 from the lysates of transfected HEK293T cells (Fig. 4E). As a control, the third intracellular loop (IL3) of GPR39 (GPR39-IL3) did not interact with GlyR α1 (Fig. 4E).

G protein–independent reversal by GPR39 of inflammation-induced glycinergic disinhibition

CFA injection reduces spinal cord glycinergic neurotransmission that subserves the inflammatory pain (*39*). Given the intimate relationship between GPR39 and GlyRs, we wanted to know if GPR39 played a role in glycinergic disinhibition after peripheral inflammation. In acute spinal slices prepared from SOM-tdTomato mice at day 1 after CFA injection, bath perfusion of GPR39 agonist TC-G 1008 dose-dependently potentiated the glycinergic synaptic transmission onto SOM$^+$ neurons (Fig. 5A). This synaptic potentiation by TC-G 1008 was dependent on GPR39 because it was compromised in *GPR39*$^{-/-}$ (fig. S7A) or shRNA-GPR39–expressing mice (fig. S7B). Comparison of paired-pulse ratios of GlyR–evoked IPSCs

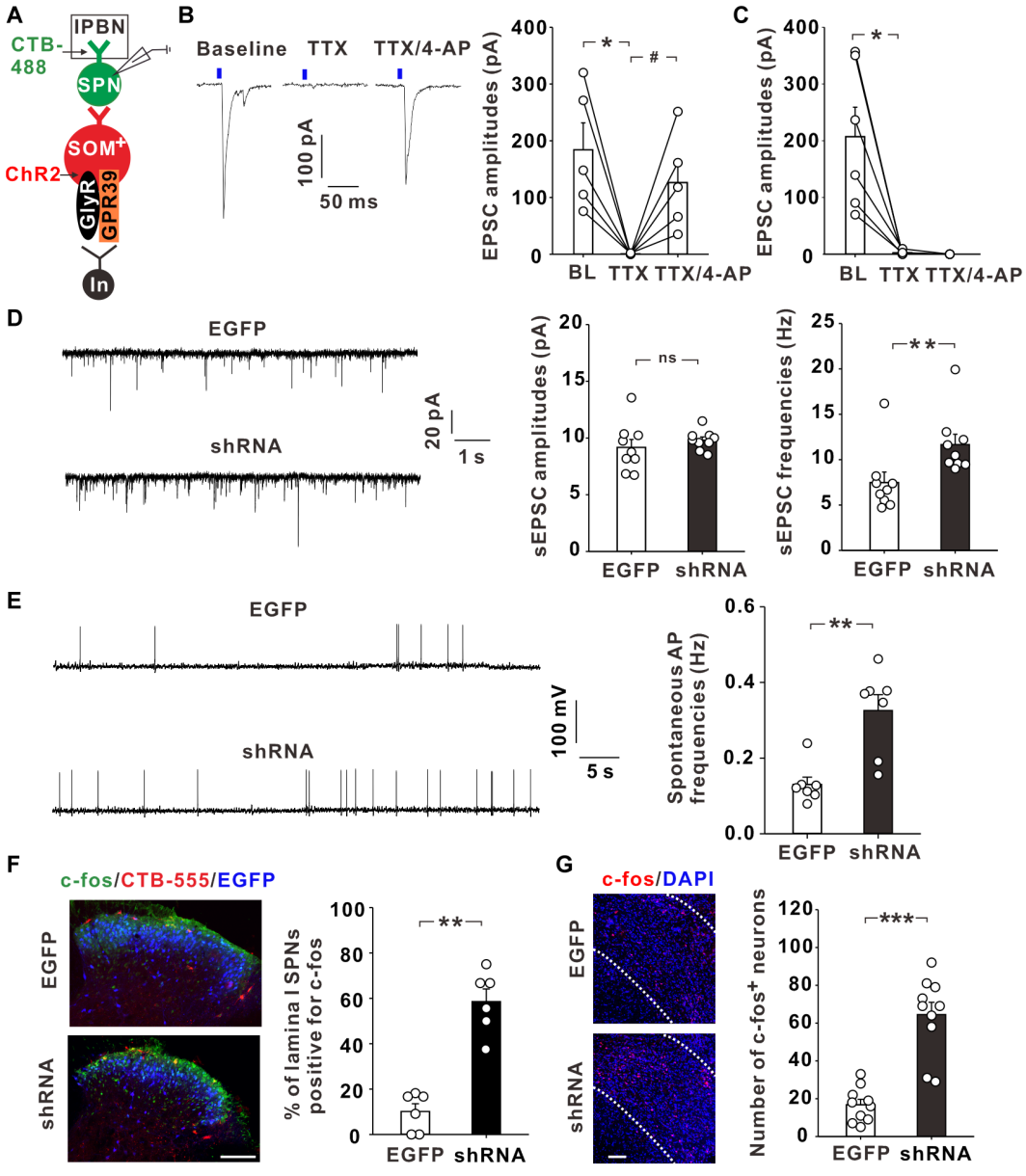

Fig. 3. GPR39 controlled the glutamatergic output from SOM$^+$ interneurons to SPNs. (**A**) Schematic of CTB-488 that was injected to the lateral PBN (IPBN) and AAV carrying ChR2 that was injected to the spinal cord of SOM-Cre mice. (**B**) Monosynaptic EPSCs evoked by blue light (473 nm, 5 mW, 2 ms, 0.1 Hz) on CTB-488–labeled SPNs before [baseline (BL)] and after sequential application of TTX (1 μM) and 4-aminopyridine (4-AP; 100 μM). *P = 0.019 and #P = 0.031 (Mann-Whitney U test). (**C**) Polysynaptic EPSCs evoked by the blue light on CTB-488–labeled SPNs. *P = 0.011 (Mann-Whitney U test). (**D**) Spontaneous EPSCs (sEPSCs) recorded on SPNs at day 21 after intraspinal injection of AAV2/9-EF1α-DIO-EGFP (EGFP) or AAV2/9-EF1α-DIO-shRNA-GPR39-EGFP (shRNA) in SOM-Cre mice. ns, P = 0.387 and **P = 0.003 (Mann-Whitney U test). n = 9 neurons from six mice per group. (**E**) Spontaneous AP firings recorded on SPNs with EGFP or shRNA expression in SOM$^+$ interneurons. **P = 0.002 (Mann-Whitney U test). n = 7 neurons from six mice per group. (**F** and **G**) Immunofluorescence for c-fos in the spinal cord (F) and IPBN (G) with EGFP or shRNA expressed in spinal SOM$^+$ interneurons of SOM-Cre mice. CTB-555 was injected in IPBN to label SPNs (red; F). **P = 0.002 and ***P < 0.001 (Mann-Whitney U test). n = 6 sections from five mice per group (F) and n = 10 sections from six mice per group (G). Scale bar, 100 μm. DAPI, 4′,6-diamidino-2-phenylindole.

(eIPSCs) showed no notable changes before and after TC-G 1008 exposure (Fig. 5B), suggesting a postsynaptic origin. This result was confirmed by immunohistochemical experiments showing that the axon terminals of spinal inhibitory neurons scarcely expressed GPR39 (fig. S8). TC-G 1008 did not affect the dorsal root–eEPSCs mediated by AMPAR and NMDAR as well as $GABA_AR$-eIPSCs (fig. S9), confirming the specificity of GPR39 in regulating GlyR responses. It was noteworthy that in the slices from naïve SOM-tdTomato mice, the activation of GPR39 by TC-G 1008 yielded negligible effects on GlyR-eIPSCs (Fig. 5C), a result in contrast to the marked decline of glycinergic currents after GPR39 knockdown (Fig. 2A). Presumably, the GPR39–GlyR α1 complex formation in the physiological state was sufficient to maintain the glycinergic inhibition.

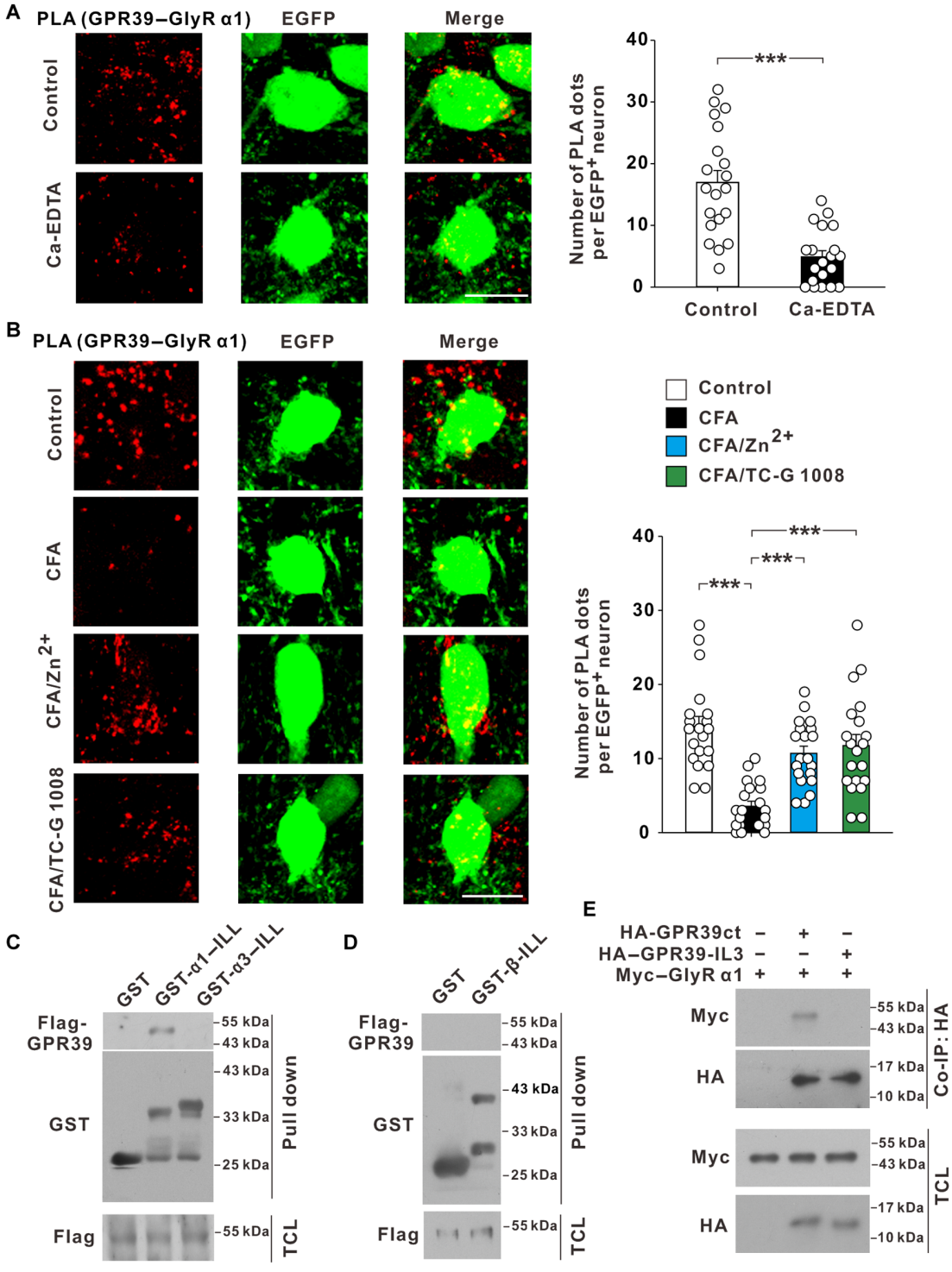

Fig. 4. Activity-dependent regulation of GPR39–GlyR α1 complex in spinal cord SOM$^+$ interneurons. (**A**) PLA detection of GPR39–GlyR α1 complex in EGFP-labeled SOM$^+$ interneurons from spinal sections of SOM-Cre mice treated with or without Ca-EDTA (25 nmol). ***$P < 0.001$ (Mann-Whitney *U* test). $n = 20$ neurons from three mice per group. Scale bar, 10 μm. (**B**) PLA detection of GPR39–GlyR α1 complex in spinal sections from control or CFA-injected SOM-Cre mice that were pretreated with intrathecal Zn^{2+} (20 nmol) or TC-G 1008 (50 pmol). ***$P < 0.001$ (Kruskal-Wallis test). $n = 20$ neurons from three to four mice per group. Scale bar, 10 μm. (**C**) GST-fused ILL of GlyR α1 (GST α1–ILL) pulled down Flag-tagged GPR39 (Flag-GPR39) from transfected HEK293T cells. GST-fused ILL of GlyR α3 (GST-α3–ILL) was used as control. Total cell lysates (TCLs) were immunoblotted for Flag. $n = 3$ experiments. (**D**) GST-fused ILL of GlyR β (GST-β-ILL) did not pull down Flag-GPR39. $n = 3$ experiments. (**E**) HA-tagged extreme C-terminal tail of GPR39 (HA-GPR39ct), but not the third intracellular loop (IL3) of GPR39 (HA–GPR39-IL3), co-immunoprecipitated (co-IP) Myc-tagged GlyR α1 from transfected HEK293T cells. $n = 3$ experiments.

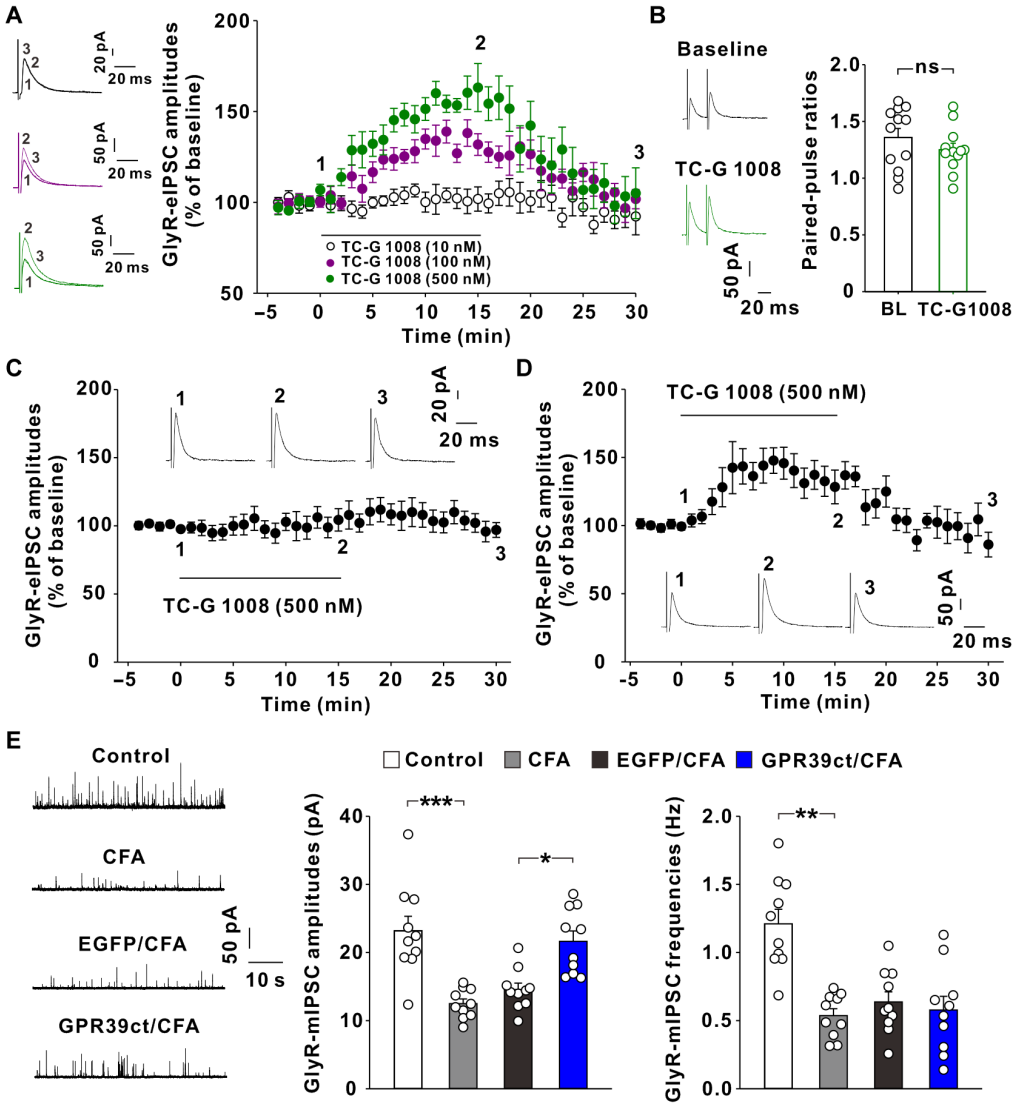

Fig. 5. Activation of GPR39 potentiated glycinergic transmission in CFA-injected SOM-tdTomato mice. (**A**) Effects of TC-G 1008 on GlyR-eIPSCs recorded on SOM$^+$ interneurons at day 1 after CFA injection (10- to 15-min post-drug: 10 nM, 101.7 ± 4.4% of baseline, $t_{11} = 0.25$, $P = 0.807$; 100 nM, 134.2 ± 4.4% of baseline, $t_{11} = 6.711$, $P < 0.001$; 500 nM, 157.1 ± 4.7% of baseline, $t_{11} = 10.836$, $P < 0.001$; paired Student's *t* test, $n = 12$ neurons per group). The horizontal bar indicated the period of TC-G 1008 perfusion. The original traces were taken at the time points indicated by the numbers 1 to 3. (**B**) Effects of TC-G 1008 (500 nM) on the paired-pulse ratios of GlyR-eIPSCs recorded at day 1 after CFA injection. $t_{11} = 1.312$; ns, $P = 0.216$ (paired Student's *t* test). $n = 12$ neurons. (**C**) TC-G 1008 did not affect GlyR-eIPSCs in spinal slices from naïve SOM-tdTomato mice (10- to 15-min post-drug: 101.8 ± 7.7% of baseline, $t_9 = 0.533$, $P = 0.607$, paired Student's *t* test, $n = 10$ neurons). (**D**) TC-G 1008 potentiated GlyR-eIPSCs in spinal slices from CFA-injected SOM-tdTomato mice when the recording pipettes contained 500 μM GDP-β-S (10- to 15-min post-drug, 135.9 ± 10.5% of baseline, $t_9 = 3.76$, $P = 0.004$, paired Student's *t* test, $n = 10$ neurons). (**E**) Viral expression of GPR39ct in SOM$^+$ interneurons blocked the decrease of GlyR-mIPSC amplitudes induced by CFA. ***$P < 0.001$, **$P = 0.002$, and *$P = 0.033$ (one-way ANOVA and post hoc Bonferroni test). $n = 10$ neurons per group.

GPR39 signals through several G proteins to a wide range of signaling cascades that generate metabolic cellular responses (*24*, *25*). To test if G protein signalings were necessary for GPR39 to potentiate the glycinergic responses, we blocked G proteins by loading nonhydrolyzable guanosine diphosphate (GDP) analog guanosine 5′-*O*-(2′-thiodiphosphate) (GDP-β-S) (500 μM) through the recording pipettes to SOM$^+$ interneurons of CFA-injected SOM-tdTomato mice. The results showed that GDP-β-S failed to block TC-G 1008 from increasing the amplitudes of GlyR-eIPSCs (Fig. 5D). Glycinergic potentiation was also elicited by TC-G 1008 when the downstream effectors of $G_{q/11}$, G_s, or $G_{12/13}$ were manipulated by intracellular loading of phospholipase C inhibitor U73122 (10 μM), PKC inhibitor chelerythrine (10 μM), phosphatidylinositol 3-kinase inhibitor wortmannin (0.2 μM), mitogen-activated protein kinase kinase inhibitor U-0126 (5 μM), cyclic adenosine 3′,5′-monophosphate–dependent protein kinase inhibitor H-89 (5 μM), or Rho-associated protein kinase inhibitor Y-27632 (10 μM; fig. S10, A to F). GPR39 activation can induce intracellular Ca^{2+} release to trigger metabotropic pathways (*40*). Nevertheless, the chelation of intracellular Ca^{2+} with 1,2-bis(2-aminophenoxy) ethane-*N*,*N*,*N*′,*N*′-tetraacetic acid (BAPTA) (10 mM) did not prevent

the potentiation of GlyR-eIPSCs by TC-G 1008 (fig. S10G). Viral expression of Gβγ sequester, the C-terminal tail of β-adrenergic receptor kinase (βARK1ct), also failed to prevent TC-G 1008 from augmenting GlyR-eIPSCs (fig. S10H). These results suggested that the G protein signalings were dispersible for GPR39 to regulate the glycinergic currents.

Our GST pull down assays have detected that the extreme carboxyl tail of GPR39 mediated the binding to GlyR α1 (Fig. 4E). On the basis of the observations that CFA-induced dissociation of GPR39–GlyR α1 complex (Fig. 4B) correlated with glycinergic disinhibition and that TC-G 1008 treatment in CFA mice resumed the complex formation (Fig. 4B) and glycinergic transmission (Fig. 5A), we assumed that this direct complex formation might regulate the glycinergic currents. To test this hypothesis, we infused a Cre-inducible AAV carrying the extreme carboxyl tail of GPR39 (AAV2/9-EF1α-DIO-GPR39ct-EGFP) to the dorsal horn of SOM-tdTomato mice (fig. S11) before CFA injection. Electrophysiological recordings on SOM^+ interneurons showed that peripheral inflammation decreased both the amplitudes and frequencies of GlyR-mIPSCs (Fig. 5E). Viral expression of GPR39ct polypeptide enhanced the amplitudes of GlyR-mIPSCs, with the frequencies left unaltered (Fig. 5E). These data corroborated that GPR39 regulated glycinergic synaptic transmission through direct interaction with GlyRs rather than G protein signalings.

Modulation of GlyR α1 tyrosine phosphorylation by GPR39

The GPR39ct polypeptide interacted directly with the ILL of GlyR α1, a structural motif that harbors putative phosphorylation residues implicated in the activity-dependent modification of glycinergic efficacy (*34*, *41*). Although a series of serine/threonine protein kinases were negligible for GPR39 to potentiate the glycinergic currents (fig. S10, A to F), we observed a marked decrease of GlyR α1 tyrosine phosphorylation in spinal cord dorsal horn of *GPR39*$^{-/-}$ mice relative to WT controls (Fig. 6A). A tyrosine residue (Tyr^{339}) within the ILL of GlyR α1 was the unique site for tyrosine phosphorylation because mutation of Tyr^{339} to phenylalanine [GlyR α1(Y339F)] completely abolished the phosphorylation signals (Fig. 6B). In HEK293T cells cotransfected with GPR39 and GlyR α1, TC-G 1008 treatment significantly potentiated the whole-cell currents evoked by puff applied glycine (Fig. 6C). This potentiation was, however, eliminated by Tyr^{339} mutation (Fig. 6C), suggesting that Tyr^{339} phosphorylation represented a key mechanism for GPR39 to enhance GlyR α1 currents.

To examine the tyrosine phosphorylation of GlyR α1 in SOM^+ interneurons, we performed in situ PLA assay in spinal sections using a pair of antibodies against GlyR α1 and phosphotyrosine (PY20). The SOM^+ interneurons were labeled by injecting AAV2/9-EF1α-DIO-EGFP into the lumbar spinal cords of SOM-Cre mice. The fluorescent PLA signals appeared as discrete puncta within EGFP-positive neurons (Fig. 6D). No signals were detected when GlyR α1 antibody was omitted (fig. S5B), suggesting the specificity of PLA detection of the phosphotyrosine residue on GlyR α1. The tyrosine phosphorylation of GlyR α1 required the presence of GPR39 because the PLA (GlyR α1 + PY20) puncta were substantially reduced when GPR39 was knocked down by viral expression of shRNA-GPR39 in SOM^+ interneurons (Fig. 6D).

To test whether GPR39 maintained GlyR α1 tyrosine phosphorylation through direct interaction, we disrupted GPR39–GlyR α1 complex by intraplantar CFA injection that preserved the expression level of each protein (fig. S6). One day after CFA injection, the number of PLA (GlyR α1 + PY20) puncta in SOM^+ interneurons declined sharply in comparison to saline control (Fig. 6E). The GPR39ct polypeptide, when expressed in SOM^+ interneurons, blocked the decline of PLA signals (Fig. 6E), suggesting that the intracellular carboxyl tail of GPR39 was sufficient to prevent GlyR α1 from dephosphorylation.

A number of protein tyrosine phosphatases (PTPs) have been detected in spinal cord dorsal horn, which contribute to the development of pathological pain (*42*, *43*). We assumed that the functional significance of GPR39–GlyR α1 complex formation was likely to block PTPs from dephosphorylating GlyR α1. The PLA assays showed that spinal treatment with PTP inhibitor Bpv (phen) reversed the decrease of GlyR α1 tyrosine phosphorylation caused by GPR39 knockdown (Fig. 6D), suggesting that GPR39 deficiency enabled PTPs to catalyze GlyR α1 dephosphorylation. In support of this, the Bpv treatment rescued the glycinergic transmission on SOM^+ interneurons (Fig. 6F) and suppressed the spontaneous licking behavior caused by GPR39 knockdown (Fig. 6G).

Inhibition of mechanical pain by enhanced GPR39 activity

To test if the reinstatement of glycinergic inhibition by GPR39 activation correlated with the pain relief, we carried out a series of behavioral assessments in CFA mice. Intrathecal application of TC-G 1008 for 60 min elevated the reflexive withdrawal thresholds (Fig. 7A) and mitigated the guarding, licking and escape behaviors evoked by von Frey filament application in CFA mice (Fig. 7B). TC-G 1008 also attenuated the dynamic inflammatory allodynia, as tested by brush stroking of the plantar surfaces of hindpaws (Fig. 7C). The hypersensitivity of inflamed mice to heat or cold stimulation was refractory to TC-G 1008 treatment (fig. S12).

We next examined the effect of TC-G 1008 on spontaneous pain, which was manifest as voluntary licking of the CFA-injected paws (Fig. 7D). TC-G 1008 (50 pmol), when spinally applied for 60 min, significantly attenuated the spontaneous licking behavior (Fig. 7D). The influence of GPR39 on pain aversion was evaluated in a conditioned place preference (CPP) paradigm. A single TC-G 1008 delivery to the spinal cords of inflamed mice drove preference for the drug-paired chamber, whereas spinal saline treatment lacked this effect (Fig. 7E). These data suggested that GPR39 activation attenuated the tonic aversive state of inflamed mice. Different from the CFA mice, the naïve mice showed no preference for the chamber paired with TC-G 1008 (fig. S13).

Clinically, the neuropathic pain is more difficult to treat than inflammatory pain. We then tested whether TC-G 1008 had an analgesic action in the spared nerve injury (SNI) model of neuropathic pain. Our data showed that intrathecal application of TC-G 1008 elevated the paw withdrawal thresholds (fig. S14A) and inhibited the attending and escape behaviors (fig. S14B) of SNI mice in response to von Frey filament stimuli. The dynamic mechanical allodynia induced by nerve injury was also alleviated by TC-G 1008 (fig. S14C). The SNI mice exhibited less spontaneous licking behavior after TC-G 1008 treatment (fig. S14D). The CPP assay demonstrated that the neuropathic mice showed preference for the chamber paired with TC-G 1008 (fig. S14E), suggesting that activation of GPR39 alleviated the ongoing pain in the context of nerve injury.

Given that GPR39 modulated the glycinergic inhibition through its extreme carboxyl tail, we tested if intracellular delivery of GPR39ct polypeptide into SOM$^+$ interneurons was able to generate a similar analgesic action as TC-G 1008. The results showed that prior expression of GPR39ct attenuated the spontaneous licking behavior induced by CFA in SOM-Cre mice (Fig. 7F). In the von Frey test, GPR39ct prevented the reduction of the reflexive thresholds induced by CFA (Fig. 7G). The attending and escape behaviors evoked by von Frey filaments were also less prominent when GPR39ct was expressed before CFA injection (Fig. 7H). We next examined the inflammatory dynamic allodynia and found that GPR39ct inhibited the guarding and licking behaviors of CFA mice to the brush stimuli (Fig. 7I). The CPA assays showed that the gentle brush stroking was aversive to the CFA-injected mice because they spent less time in the chamber where the repetitive brushings were applied (Fig. 7J). Prior expression of GPR39ct reduced avoidance of the brush-paired chamber (Fig. 7J), suggesting that the intracellular carboxyl tail of GPR39 alone was sufficient to inhibit the light touch-evoked unpleasant aversive feeling. These data also supported the notion

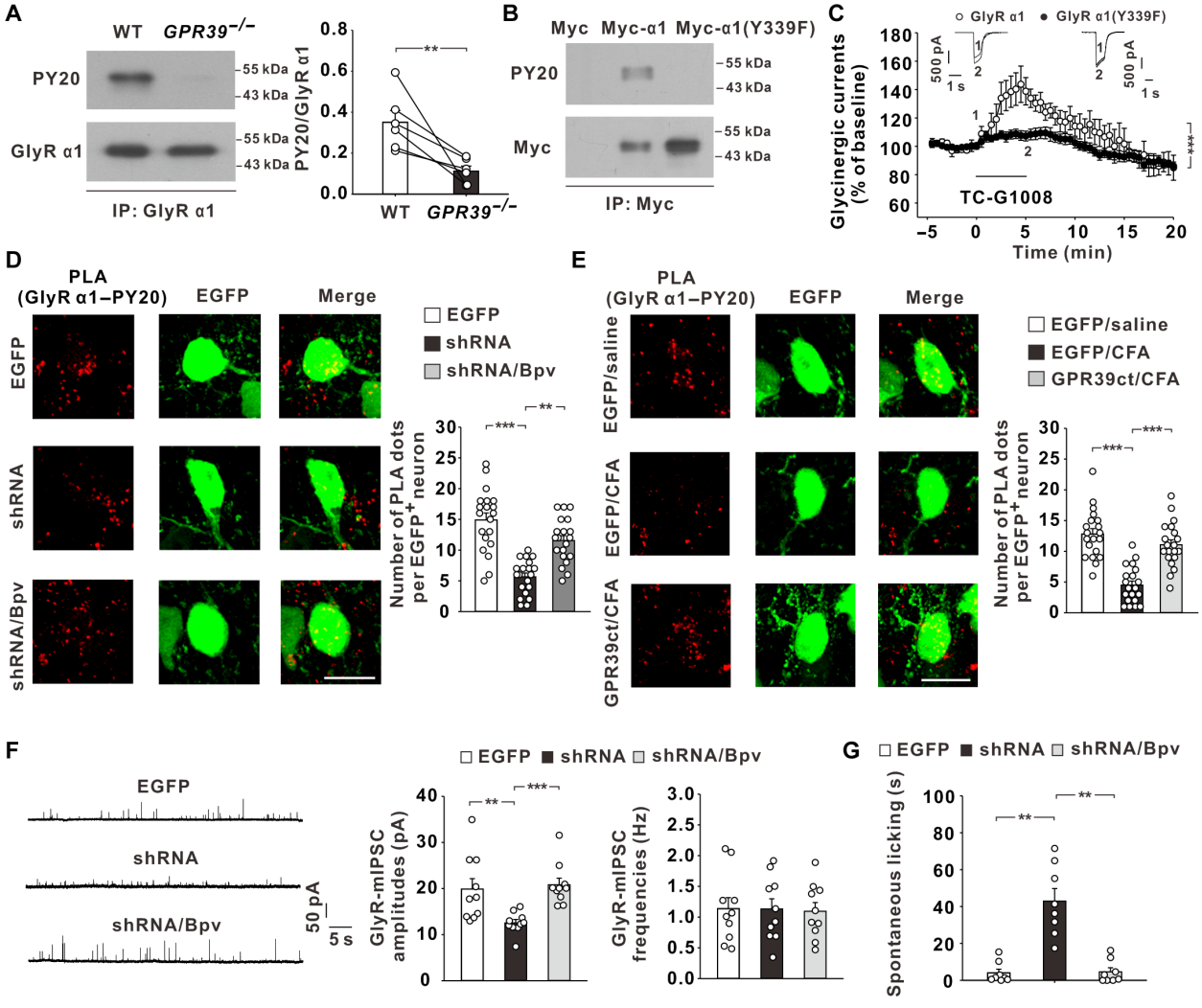

Fig. 6. GPR39 maintained the tyrosine phosphorylation of GlyR α1. (**A**) GlyR α1 immunoprecipitates (IP) from spinal cord dorsal horns of WT and *GPR39*$^{-/-}$ mice were immunoblotted with phosphotyrosine (PY20) antibody and GlyR α1 antibody. $^{**}P = 0.002$ (Mann-Whitney *U* test). $n = 6$ experiments. (**B**) Myc immunoprecipitates from HEK293T cells expressing Myc-tagged GlyR α1 (Myc-α1) or GlyR α1(Y339F) mutant [Myc-α1(Y339F)] were immunoblotted with PY20 and Myc antibody. $n = 3$ experiments. (**C**) Effects of bath TC-G 1008 perfusion (500 nM; horizontal bar) on glycine (1 mM, 10 ms)-evoked whole-cell currents in HEK293T cells coexpressing GPR39 and GlyR α1 or GlyR α1(Y339F). The original traces were taken at the time points indicated by the numbers 1 and 2. $F_{49,882} = 2.67$, $^{***}P < 0.001$ (repeated measurement). $n = 10$ cells per group. (**D**) PLA assay of GlyR α1 tyrosine phosphorylation with a pair of PY20 and GlyR α1 antibody in spinal SOM$^+$ interneurons transfected with AAV2/9-EF1α-DIO-EGFP (EGFP) or AAV2/9-EF1α-DIO-shRNA-GPR39-EGFP (shRNA). Bpv (5 nmol) was spinally applied for 30 min before PLA assay. $^{**}P = 0.001$ and $^{***}P < 0.001$ (Kruskal-Wallis test). $n = 20$ cells from four mice per group. Scale bar, 10 μm. (**E**) PLA assay of GlyR α1 tyrosine phosphorylation in SOM$^+$ interneurons expressing EGFP or GPR39ct at day 1 after saline or CFA injection. $^{***}P < 0.001$ (Kruskal-Wallis test). $n = 20$ cells from three to four mice per group. Scale bar, 10 μm. (**F**) Effect of bath Bpv (100 μM) perfusion on GlyR-mIPSCs recorded on spinal SOM$^+$ interneurons expressing shRNA. $^{**}P = 0.008$ and $^{***}P < 0.001$ (Kruskal-Wallis test). $n = 10$ neurons from six mice per group. (**G**) Intrathecal application of Bpv (5 nmol) attenuated spontaneous licking behavior in SOM-Cre mice with spinal SOM$^+$ interneurons expressing shRNA. $^{**}P = 0.002$ (Kruskal-Wallis test). $n = 8$ mice per group.

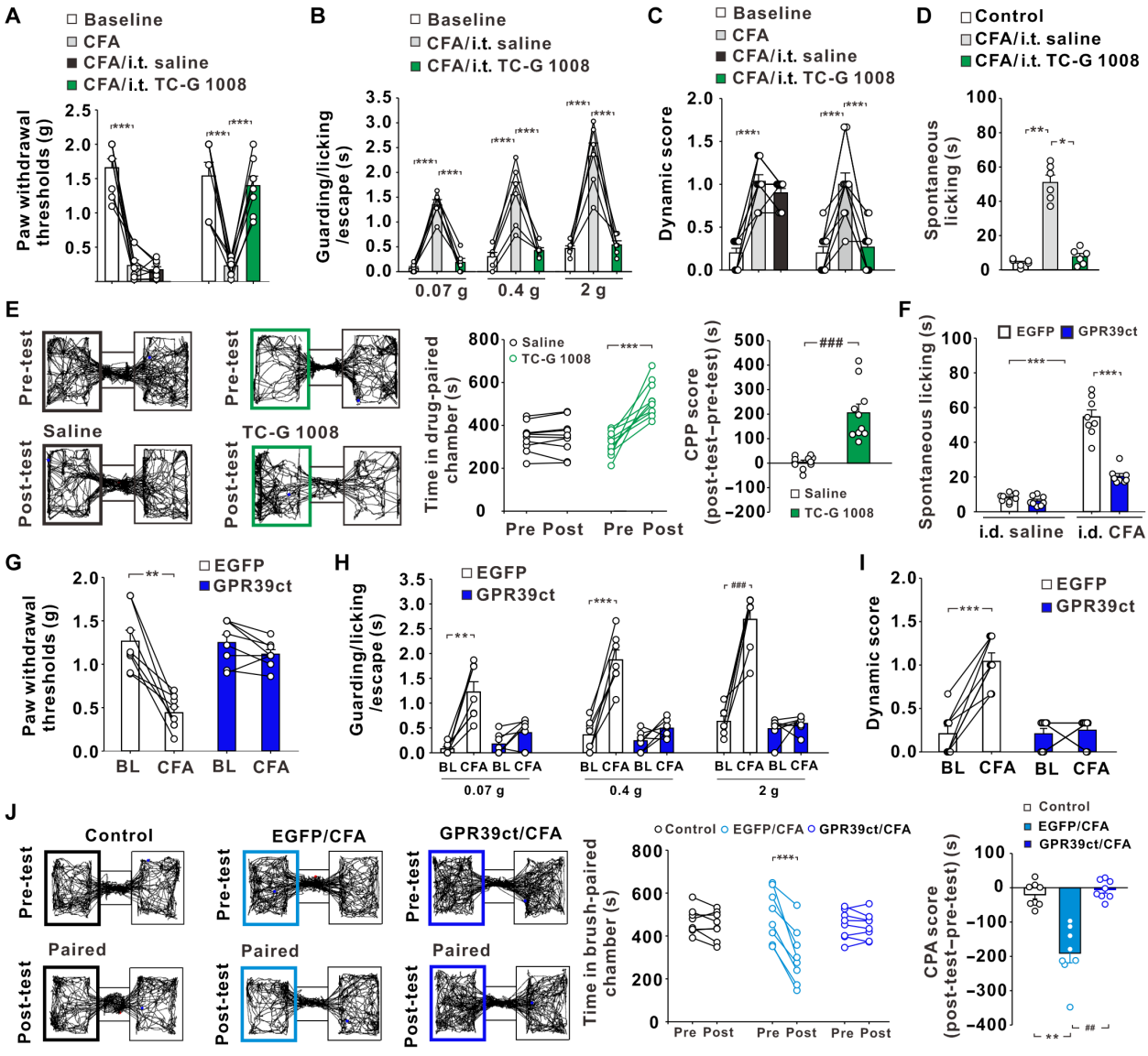

Fig. 7. TC-G 1008 and GPR39ct polypeptide inhibited inflammatory mechanical pain. (**A**) Intrathecal (i.t.) application of TC-G 1008 (50 pmol) for 60-min attenuated punctate mechanical allodynia in CFA mice. ***$P < 0.001$ (one-way ANOVA followed by post hoc Bonferroni test). $n = 8$ mice per group. (**B** and **C**) TC-G 1008 inhibited the attending/escape behaviors to von Frey filament stimuli (B) and dynamic mechanical allodynia to brush stimuli (C) at day 1 after CFA injection. ***$P < 0.001$ (one-way ANOVA followed by post hoc Bonferroni test). $n = 6$ (B) and 10 mice per group (C). (**D**) Spontaneous licking activities of mice. *$P = 0.039$ and **$P = 0.002$ (Kruskal-Wallis test). $n = 6$ mice per group. (**E**) TC-G 1008 (50 pmol) induced CPP in CFA mice. ***$P < 0.001$ ($t_9 = 5.722$, paired Student's t test) and ###$P < 0.001$ (Mann-Whitney U test). $n = 10$ mice per group. (**F**) Spontaneous licking activities 1 day after intradermal (i.d.) saline or CFA injection in SOM-Cre mice expressing EGFP or GPR39ct. ***$P < 0.001$ (one-way ANOVA and post hoc Bonferroni test). $n = 8$ mice per group. (**G**) von Frey thresholds before and after CFA injection. $t_7 = 5.328$, **$P = 0.001$ (paired Student's t test). $n = 8$ mice per group. (**H**) Attending and escape behaviors to von Frey filament stimuli before and after CFA injection. $t_6 = 5.44$, **$P = 0.002$; $t_6 = 8.23$, ***$P < 0.001$; $t_6 = 7.276$, ###$P < 0.001$ (paired Student's t test). $n = 7$ mice per group. (**I**) Brush-evoked pain responses. $t_7 = 7.638$, ***$P < 0.001$ (paired Student's t test). $n = 8$ mice per group. (**J**) Brushing evoked CPA in inflamed SOM-Cre mice with spinal SOM$^+$ interneurons expressing EGFP but not GPR39ct. ***$P < 0.001$ ($t_7 = 6.78$, paired Student's t test), **$P = 0.005$, and ##$P = 0.001$ (Kruskal-Wallis test). $n = 8$ mice per group.

that G protein signalings were dispersible for GPR39 to regulate mechanical pain. Viral expression of GPR39ct did not inhibit the heat and cold hypersensitivities in the CFA mice (fig. S15). In summary, our data unraveled an important role of GPR39 in the feedforward glycinergic inhibition of spinal cord SOM$^+$ interneurons, a key subpopulation in the neural circuits associated with both the sensory discriminative and affective motivational aspects of chronic pain.

DISCUSSION

The spinal cord dorsal horn is a critical hub that drives defensive reflexive responses to noxious stimuli and transmits the nociceptive information to a set of brain structures for the generation of pain aversiveness. The current study found that: (i) GPR39, a unique Zn^{2+}-sensitive G protein–coupled receptor (*44*), was expressed in spinal cord SOM$^+$ interneurons and distributed at inhibitory postsynaptic sites, where GPR39 directly complexed with GlyRs and was

integral to normal glycinergic inhibition; (ii) GPR39 controlled the excitatory glutamatergic output from SOM^+ interneurons to spinoparabrachial projection neurons that engage the superspinal neural circuits encoding both the defensive and affective domains of pain. Our data showed that at the spinal level, the targeted manipulation of GPR39 activity or GPR39-GlyR complex formation in SOM^+ interneurons effectively mitigated the multidimensional experience of inflammatory and neuropathic pain.

Heteromerization between G protein–coupled receptors and ion channels on the plasma membrane has been proposed as an officious way to achieve a diversity of cellular functional modifications (*45*–*48*). Previous studies have revealed a Zn^{2+}-driven interaction of GPR39 with 5-hydroxytryptamine receptor 1A (5-HT1A) (*46*, *48*). The 5-HT1A–GPR39 oligomer is implicated to integrate the zincergic and serotonergic signalings with a potential for the treatment of depression (*46*, *48*). The current study identified ionotropic GlyR α1 as another binding partner of GPR39 and provided evidence that GPR39–GlyR α1 complex were necessary for the glycinergic inhibition of SOM^+ interneurons. Mechanistically, the intracellular carboxyl region of GPR39 was found to prevent GlyR α1 from tyrosine dephosphorylation, possibly by concealing the phosphotyrosine residue on GlyR α1 or impeding PTP access to GlyR α1. Activation of GPR39 in the spinal cord of intact mice generated no change of glycinergic strength, suggesting that the interaction between GPR39 and GlyR α1 might be saturated under resting conditions. Deletion of GPR39 led to GlyR α1 dephosphorylation and glycinergic disinhibition, suggesting an important role of GPR39–GlyR α1 complex in the stabilization of normal glycinergic transmission. The identities of PTPs targeting GlyR dephosphorylation require further investigation.

Zn^{2+} has been shown to inhibit pain perception in many pain models (*16*, *17*). As an allosteric modulator of GlyR α1, extracellular Zn^{2+} dynamically regulates the apparent affinity of glycine for the chloride channel (*30*, *49*). Accumulating evidence has indicated that Zn^{2+} also stimulates the conformational change of GPR39 and is widely considered as an endogenous ligand for GPR39 (*44*, *50*). Here, we found an important role of Zn^{2+} in driving the complex formation between GPR39 and GlyR α1. It was reasonable that Zn^{2+} might accomplish the regulatory effects on glycinergic transmission through two pathways: the direct binding to GlyR α1 for allosteric modulation of the channel properties and the indirect binding to GPR39 for metabolic modulation of GlyR α1 tyrosine phosphorylation, both of which might be necessary for normal glycinergic inhibition.

As a critical component of spinal mechanosensory circuits, most of the SOM^+ lineage excitatory neurons are confined to lamina II that segregates the deeper LTMR-recipient zone and superficial nociceptive projection neurons (*10*, *51*). Primary afferent LTMRs synapse onto SOM^+ interneurons and drive a dense feedforward inhibition (*10*). Ablation of SOM^+ population diminishes the reflexive withdrawal responses to light touch (*10*). In contrast, optogenetic stimulation of SOM^+ interneurons in naïve mice causes a CPA, which correlates with the induction of c-fos in spinal neurokinin 1 receptor–positive projection neurons (*9*). These results suggest that SOM^+ interneurons are dedicated to relaying mechanosensory signals to superspinal structures. The lateral parabrachial nuclei are established to receive inputs from molecularly distinct spinal projection neurons and contribute to the defensive jumping, recuperative licking, and pain aversive learning by engaging several downstream brain subregions (*12*–*15*). The current study showed that SOM^+ interneurons engaged lamina I SPNs, a monosynaptic or polysynaptic connection that might transmit the low-threshold mechanosensory inputs to pain affect–processing brain nuclei. This connection was silent under physiological conditions partly due to strong feedforward glycinergic inhibitory control, a synaptic event that required GPR39 activity. In the absence of GPR39, the light touch became aversive and caused the pain perception and affect. It is worthwhile to mention that GPR39 was also present out of inhibitory synapses. Although the pain behaviors observed after knockdown of GPR39 in SOM^+ neurons correlated closely with glycinergic synaptic disinhibition, additional studies are warranted to examine whether GPR39 outside the inhibitory synapses also plays a role in the pain modification.

Together, our data suggested that Zn^{2+}-sensitive GPR39 at the spinal level represented a promising target for the treatment of mechanical pain, both in the reflexive defensive and affective motivational aspects.

MATERIALS AND METHODS

Animals and pain models

All experimental procedures were approved by the Institutional Animal Care and Use Committee of Lanzhou University. The male adult C57BL/6J mice (8 to 10 weeks) were purchased from the Experimental Animal Center of Lanzhou University (approval number: SCXK (GAN)-2013-0002). The *GPR39* knockout mice (KOCMP-00773) were purchased from Cyagen Bioscience (Suzhou, China). The B6.Cg-*Gt(ROSA)26Sor*$^{tm9(CAG\text{-}tdTomato)Hze}$/J (Ai9) reporter mice (JAX 007909), *SST*$^{tm2.1(cre)Zjh}$/J (SOM-Cre) mice (JAX 013044) and B6J.129S6(FVB)-*Slc32a1*$^{tm2(cre)Lowl}$/MwarJ (vGAT-cre) mice (JAX 028862) were obtained from the Jackson Laboratory. The SOM-Cre and Ai9 mice were crossed to label SOM^+ neurons with tdTomato. The animals were housed on a 12-hour light/12-hour dark cycle with free access to water and food and were assigned randomly to experimental groups. The inflammatory pain was induced by subcutaneous injection of CFA (20 μl; Sigma-Aldrich) into the plantar surfaces of hindpaws. To establish the SNI model of neuropathic pain, we anesthetized the mice by intraperitoneal injection of sodium pentobarbital (90 to 120 mg/kg) and exposed the left sciatic nerve. The tibial and common peroneal nerves were tightly ligated and severed distal to the ligation, followed by removing a 2- to 3-mm portion of each nerve. The sural branch of the sciatic nerve was left intact during the operation (*39*). The sham surgery was conducted by exposing the sciatic nerve without any nerve injury. The muscle and skin were then closed in layers.

Virus, expression constructs, and reagents

The AAV2/9-EF1α-DIO-GPR39ct-EGFP (2.0×10^{12} vg/ml), AAV2/9-EF1α-DIO-EGFP (2.0×10^{12} vg/ml), and AAV2/9-hSyn-DIO-Synaptophysin-mCherry (2.45×10^{12} vg/ml) were purchased from BrainVTA (Wuhan, China). The GPR39ct polypeptide encompassed amino acids 344 to 456 of mouse GPR39. The AAV2/9-EF1α-DIO-shRNA-GPR39-EGFP (5.3×10^{13} vg/ml) was obtained from Sunbio Biomedical Technology (Shanghai, China). The sequence of shRNA-GPR39 was 5′-GATCCAAAAAAGGTGTACCTGATCATCTTTGTTCTCTTGAAACAAAG ATGATCAGGTACACC-3′. The AAV2/9-EF1α-DIO-ChR2(H134R)-mCherry (3.2×10^{12} vg/ml) was purchased from BrainCase (Shenzhen, China). The pRK5-BARK1 plasmid was a gift from R. Lefkowitz (Addgene #14695). We obtained the recombinant adenovirus (10^{10} plaque-forming units/ml) encoding EGFP and BARK1 from Yingrun Biotechnologies (Changsha, China).

The full-length mouse GlyR α1 cDNA, human GlyR α3, and GlyR β cDNAs in pcDNA3.1 vector were obtained from Youbio Biotechnologies (Changsha, China). The site-directed mutagenesis was used to generate GlyR α1(Y339F) (the number did not include the signal peptide sequence). The isolated GlyR α1 or GlyR α1(Y339F) cDNA was modified by inserting c-Myc sequence (EQKLISEEDL) between the second and third amino acids (*39*). The ILL of human GlyR α1 (residues 308 to 392), GlyR α3 (residues 308 to 400), or GlyR β (residues 329 to 456) was polymerase chain reaction (PCR)–subcloned and ligated into pGEX-6p-1 vector (*39*). The full-length human GPR39 cDNA in pcDNA3.1 or pcDNA3.1-Flag vector was obtained from Youbio Biotechnologies. The extreme carboxyl terminus (residues 344 to 453) and the IL3 (residues 245 to 281) of human GPR39 were PCR-subcloned and ligated into pcDNA3.1–hemagglutinin (HA) vector. All constructs were verified by DNA sequencing.

TC-G 1008 (Sigma-Aldrich), chelerythrine (Sigma-Aldrich), wortmannin (Sigma-Aldrich), U-0126 (Sigma-Aldrich), H-89 (Sigma-Aldrich), and U-73122 (Absin, Shanghai, China) were dissolved in dimethyl sulfoxide, which were diluted with saline or internal solution before use. The final concentration of dimethyl sulfoxide was less than 0.5%. GDP-β-S (Sigma-Aldrich), Bpv(phen) [potassium bisperoxo (1,10-phenanthroline) oxovanadate (V); Calbiochem, MA, USA], TTX (Absin), 4-aminopyridine (Absin), Ca-EDTA (Absin), Y-27632 (Absin) and BAPTA (Absin), bicuculline (Sigma-Aldrich), strychnine (Sigma-Aldrich), 6-Cyano-7-nitroquinoxaline-2,3-dione (CNQX; Sigma-Aldrich), and D(-)-2-amino-5-phosphonopentanoic acid (D-APV; Sigma-Aldrich) were dissolved in saline, external, or internal solution.

Stereotaxic injection and drug delivery

Intraspinal viral injection was performed in 3- to 4-week-old mice for electrophysiological recordings or in 5- to 7-week-old mice for other experiments. In brief, the mice were anesthetized by intraperitoneal injection of sodium pentobarbital (90 to 120 mg/kg) and mounted on a stereotaxic frame after a laminectomy (*39*, *52*). A glass pipette filled with the viral vector was attached to a microsyringe pump (R-480, RWD, Shenzhen, China). The pipette tip (40 μm in diameter) was positioned at a depth of 0.2 to 0.3 mm from the dorsal surface of L4-L5 lumbar segment and 0.5 mm apart from the midline for viral injection (300 nl, 30 nl/min). We conducted three unilateral injections (0.5 mm apart) in each mouse. After the injection, the muscle and skin were closed. The experiments were conducted after 21-day recovery.

For fluorescent retrobead labeling with CTB-488 (Invitrogen) or CTB-555 (Invitrogen), a midline incision was made to expose the cranium and a hand-held drill was used to create a burr hole through which a glass pipette was inserted to the lateral parabrachial nuclei (anterior-posterior, −5.1 mm; medial-lateral, ±1.2 mm; dorsoventral, −3.35 mm). The retrobead (1%, 50 nl) was injected slowly through a microsyringe pump. After the injection, the pipette was left in place for 5 to 10 min before being withdrawn. Intrathecal drug injection (5 μl) was achieved by direct lumbar puncture as described previously (*39*, *52*).

Behavioral tests

All behavioral tests were conducted blindly. The mice were habituated to the testing environment for 30 min on three consecutive days before baseline measurements. For von Frey test, the mice were placed in a chamber with metal mesh floor, and a series of von Frey filaments were applied perpendicularly to the plantar surfaces of hindpaws. The 50% paw withdrawal thresholds were calculated by using up-down method (*52*). To assess the attending and escape behaviors evoked by the punctate force, we sequentially applied three von Frey filaments (0.07, 0.4, and 2 g) to the plantar surfaces of hindpaws. Each filament was used only once, and the time spent by the mice on the escape and attending of the stimulated paws was videotaped and calculated within 30 s after each filament application (*53*). To measure the dynamic mechanical sensitivity, a custom-made paintbrush (5 mm in length) was used to stroke the plantar surfaces of hindpaws from heel to toe at a velocity of about 2 cm/s. The responses of mice were scored according to previous reports (*11*): Score 0, a fast movement or lifting of the stimulated paws; score 1, a sustained lifting (more than 2 s) or single flinching of the stimulated paws; score 2, a strong lateral lifting of the stimulated paws or a startle-like jumping; score 3, multiple flinching or licking of the stimulated paws. The brushing stimuli were delivered for three times (3-min interval) to obtain the averaged score (*10*). In the Hargreaves test, the mice were placed on a transparent glass plate and a beam of light was delivered to the plantar surfaces of hindpaws to measure the paw withdrawal latencies. We set a cutoff time of 10 s to avoid the tissue damage (*39*). For the measurement of cold sensitivity, a drop of acetone was dabbed onto the plantar surfaces of hindpaws through a syringe that did not touch the skin. The first 10-s activities were excluded, and the time spent by the mice on flicking and licking the stimulated paws was recorded for 60 s afterward (*39*, *54*).

To assess the spontaneous pain behaviors (*55*), the mice were individually placed in a transparent PLEXIGLAS cage (18 cm by 18 by 22 cm). After 30 min of habituation, we videotaped and analyzed the total traveling distance, the mean locomotion velocity, and the time spent on licking the thighs and paws over a 30-min period.

The CPP test was performed as described previously (*56*). The CPP apparatus consisted of two chambers (18 cm by 18 cm by 22 cm) with distinct visual cues (one was decorated with dark floor and walls, and another was with white floor and walls), which were interconnected with a central neutral corridor. The CPP test was conducted 21 days after viral injection or one day after CFA injection. On the habituation day, the mice were individually placed in the central corridor with free access to both chambers for 15 min. On the pre-conditioning day, the mice were placed into the neutral corridor and allowed to explore the whole apparatus freely for 15 min. Most of the mice usually displayed a slight preference for the chamber with dark floor and walls. We analyzed the movement of mice with SuperMaze software (XinRun Information Technology, Shanghai, China) and defined the time spent in the innate nonpreferred chamber as the pre-conditioning time. The mice spending more than 80% of the total time in either chamber during the pre-conditioning session were not used for further test. During the conditioning day, the mice received intrathecal TC-G 1008 injection in the morning and were restricted to their innate nonpreferred chamber for 60 min. The control mice were administrated with saline. Four hours later, the mice received intrathecal saline injection and were restricted to their innate preferred chamber for 60 min. A single trial conditioning protocol was used in TC-G 1008 group. On the post-conditioning day, the mice were placed into the neutral corridor to roam freely through the entire apparatus for 15 min. The time spent in the drug-paired chamber was defined as the

post-conditioning time. The CPP score was calculated by subtracting the pre-conditioning time from the post-conditioning time.

In the CPA test, the three-chamber apparatus was placed on an elevated wire mesh that served as the chamber floor (*11*). On day 1, the mice were habituated to the apparatus for 15 min with free access to all the chambers. On day 2, the mice were placed into the neutral corridor and allowed to freely explore the apparatus for 15 min. Most of mice showed a slight preference for the dark chamber. We recorded the time spent in the innate preferred chamber as the pre-conditioning time. On days 3 and 5, the mice were confined to their innate preferred chamber, and a custom-made paintbrush was used to stimulate the plantar surfaces of hindpaws from heel to toe for 15 min with an interval of about 2 s. On days 4 and 6, the mice were confined to their innate nonpreferred chamber for 15 min. On day 7, the mice were placed into the neutral corridor and allowed to roam freely through the whole apparatus for 15 min. The time spent in the brushing-paired chamber was recorded as the post-conditioning time. The CPA score was calculated by the post-conditioning time minus the pre-conditioning time.

Immunohistochemistry

Mice were deeply anesthetized by intraperitoneal injection of sodium pentobarbital (90 to 120 mg/kg) and perfused through the ascending aorta with 10 ml of ice-cold phosphate-buffered saline (PBS) and 10 ml of paraformaldehyde (4%). The lumbar spinal cord, DRG, or brain was dissected out and post-fixed for 2 hours (spinal cord and DRG) or overnight (brain tissue) at 4°C in PBS containing 4% paraformaldehyde. After washes with PBS, the tissues were cryoprotected in PBS containing 30% sucrose at 4°C for 24 hours (spinal cord and DRG) or 48 hours (brain tissue) and sectioned at 40 μm in thickness on a cryostat at −20°C. The sections were blocked at 4°C with 10% normal goat serum (NGS) and 0.25% Triton X-100 in PBS overnight and then incubated with primary antibodies for 48 hours. After complete washes with PBS containing 10% NGS, the sections were incubated for 2 hours at room temperature with Alexa 488–, Cy3-, or Alexa 647–conjugated secondary antibodies (1:500; Invitrogen). Fluorescence images were captured by a confocal laser scanning microscope (SP8, Leica). The primary antibodies used in this study included the rabbit anti-GPR39 antibody (1:500; Novus Biologicals, #NLS142), mouse anti-CGRP antibody (1:1000; Sigma-Aldrich, #4901), mouse anti-GFAP antibody (1:5000; Sigma-Aldrich, #G3893), mouse anti-PKCγ antibody (1:200; Santa Cruz Biotechnology, #sc-166385), mouse anti-CD11B antibody (OX-42; 1:500; Bio-Rad, #MCA275), mouse anti-NeuN antibody (1:5000; Millipore, #MAB377), rabbit anti–c-fos antibody (1:800; Proteintech, #26192-1-P), and mouse anti-gephyrin antibody (1:200; Synaptic System, #147021). The fluorescein isothiocyanate–conjugated IB4 (1:200; Sigma-Aldrich, #L2895) was incubated for 2 hours at room temperature to label non-peptidergic C fiber nociceptors before image capture.

Proximity ligation assay

The transverse spinal slices of 40 μm in thickness were prepared as described above. Fluorescence PLA was conducted with Duolink in situ fluorescence kit (Sigma-Aldrich) according to the manufacturer's instructions (*57*–*60*). In brief, the sections were incubated for 10 min at room temperature with the antigen retrieval solution (Beyotime, #P0090). After the antigen retrieval, the sections were permeabilized with PBS containing 0.25% Triton X-100 for 12 hours, blocked for 60 min at 37°C with the Duolink blocking solution, and incubated overnight at 4°C with a mixture of rabbit anti-GPR39 (1:500; Novus Biologicals, #NLS142) and mouse anti–GlyR α1 antibody (1:200; Synaptic System, #146111) or a mixture of rabbit anti–GlyR α1 (1:200; Synaptic System, #146003) and mouse phosphotyrosine (PY) antibody (1:200; Sigma-Aldrich, #P4110). All the primary antibodies were diluted with 1× Duolink antibody diluent. After two washes with 1× wash buffer A, the sections were incubated with the Duolink In Situ PLA probe anti-rabbit PLUS (1:5) and anti-mouse MINUS (1:5) at 37°C for 60 min in a humid incubator. The remaining PLA probes were washed out with 1× wash buffer A. The ligase was diluted (1:40) with 1× ligation buffer and incubated with the sections for 30 min at 37°C in the humid incubator. After two washes with 1× wash buffer A, the sections were incubated for 100 min at 37°C with the polymerase diluted (1:80) in 1× amplification buffer in the darkened humid incubator. The sections were sequentially washed with 1× wash buffer B (2× for 10 min) and 0.01 × wash buffer B (1× for 10 min). The coverslips were mounted with Duolink In Situ mounting medium, and the fluorescence images were captured with a confocal laser scanning microscope.

GST pull-down assay, immunoprecipitation, and Western blot

GST-fused proteins were expressed in *Escherichia coli* BL21 cells and purified as previously described (*39*). The GST protein bound to glutathione agarose beads was incubated for 4 hours at 4°C with the whole-cell lysates of HEK293T cells (American Type Culture Collection, #CRL-3216) transfected with Flag-GPR39. After brief centrifugation at 800*g*, the beads were harvested, washed with the radioimmunoprecipitation assay (RIPA) buffer [50.0 mM tris•HCl (pH 8.0), 150.0 mM NaCl, 1.0 mM EDTA, 1.0% NP-40, 0.1% SDS, 0.5% sodium deoxycholate, and phosphatases/proteases inhibitor cocktail (Sigma-Aldrich)], and boiled in SDS sample buffer for immunoblotting analysis.

For immunoprecipitation, the mice were deeply anesthetized by intraperitoneal injection of sodium pentobarbital (90 to 120 mg/kg). The experimenters were blind to the experimental groups. The L4-L5 lumbar spinal cord was isolated in ice-cold artificial cerebrospinal fluid [ACSF; 119.0 mM NaCl, 2.5 mM $CaCl_2$, 2.5 mM KCl, 1.3 mM $MgCl_2$, 1.0 mM NaH_2PO_4, 26.0 mM $NaHCO_3$, and 11.0 mM D-glucose (pH 7.4), oxygenated with 95% O_2 and 5% CO_2] and homogenized in the RIPA buffer. HEK293T cells were also lysed in the RIPA buffer. Following centrifugation at 14,000*g* for 10 min, the supernatant was collected and the protein concentration was measured with the Bicinchoninic Acid Assay Kit (Beyotime, #P0012S). The supernatant was incubated with the primary antibody under gentle rotation at 4°C overnight. The immune complexes were incubated with protein A/G agarose beads at 4°C for 4 hours. Following extensive washes with the RIPA buffer, the immunoprecipitates were boiled in SDS sample buffer for 5 min for Western blot analysis.

The protein samples were separated on SDS–polyacrylamide gel electrophoresis and transferred to polyvinylidene difluoride membranes. The membranes were blocked for 30 min by 5% nonfat milk and incubated with primary antibodies overnight at 4°C. After washes with Phosphate-Buffered Saline containing Tween-20 (PBST), the membranes were incubated with horseradish peroxidase–conjugated secondary antibodies for 60 min under gentle rotation at room temperature. The protein signals were visualized with

enhanced chemiluminescence. The primary antibodies used in the present study included the rabbit anti–GlyR α1 (1:200; #146003) and mouse anti–GlyR α1 antibody (1:200; #146111) from Synaptic System, rabbit anti-GPR39 antibody (1:500; Novus Biologicals, #NLS142), mouse anti–β-actin (1:800; #A5316) and mouse phosphotyrosine (PY) antibody (1:200; #P4110) from Sigma-Aldrich, mouse anti-Flag (1:5000; #E0017) and mouse anti-GST antibody (1:20,000; #E0019) from Anbo Biotechnology (Jiangsu, China), mouse anti-HA antibody (1:1000; Proteintech, #66006-1), mouse anti-Myc antibody (1:600; Santa Cruz Biotechnology, #sc-40), and rabbit anti-Myc antibody (1:1000; Abcam, #ab9106).

Electrophysiological recordings

Electrophysiological recordings were conducted blindly by the experimenters without knowledge of the manipulations that the animals had received. The mice (6 to 7 weeks old) were deeply anesthetized by intraperitoneal injection of sodium pentobarbital (90 to 120 mg/kg). The lumbar segment of spinal cord was isolated in ice-cold sucrose solution [50.0 mM sucrose, 95.0 mM NaCl, 1.8 mM KCl, 1.2 mM NaH_2PO_4, 0.5 mM $CaCl_2$, 7.0 mM $MgCl_2$, 26.0 mM $NaHCO_3$, 15.0 mM D-glucose (pH 7.4), and oxygenated with 95% O_2 and 5% CO_2]. A transverse slice (300 μm in thickness) with or without an attached L4 or L5 dorsal root was cut on a vibratome stage. The slice was transferred to the recording chamber and perfused (5 ml/min) with oxygenated ACSF (32° to 33°C). The whole-cell patch clamp recordings were performed under an Olympus BX51WIF microscope equipped with a 40× water immersion objective under fluorescence and transmitted light illumination.

To record the inhibitory synaptic transmission, the membrane potential was held at 0 mV with an Axon 700B Amplifier in the voltage-clamp mode. The glass electrodes had the resistance of 3 to 5 megohm when filled with the internal solution [110.0 mM Cs_2SO_4, 5.0 mM KCl, 2.0 mM $MgCl_2$, 5.0 mM Na_2–adenosine 5′-triphosphate (ATP), 0.5 mM Na–guanosine 5′-triphosphate (GTP), 20.0 mM Hepes, and 0.6 mM EGTA (pH 7.25, 310 to 320 mOsm)]. The inhibitory synaptic currents were evoked by focal electrical stimulation (0.1 Hz) delivered through a glass pipette that was positioned adjacent to the recorded neurons. The glycinergic inhibitory responses were pharmacologically isolated by adding NMDAR antagonist D-APV (50 μM), AMPAR antagonist CNQX (10 μM), and $GABA_AR$ antagonist bicuculline (10 μM) in the external solution. Two successive electrical stimuli (30-ms interval) were delivered to evoke GlyR–eIPSCs and measure the paired-pulse ratios (second response/first response). The GABAergic synaptic components were pharmacologically isolated by adding GlyR antagonist strychnine (2 μM), D-APV, and CNQX in the external solution. For mIPSC recordings, 1 μM TTX was also included in the external solution.

To record the excitatory synaptic transmission, the glass pipettes were filled with the internal solution containing 115.0 mM cesium methanesulfonate, 20.0 mM CsCl, 10.0 mM Hepes, 2.5 mM $MgCl_2$, 4.0 mM Na_2-ATP, 0.4 mM Na-GTP, 0.6 mM EGTA, and 10.0 mM sodium phosphocreatine (pH 7.25, 310 to 320 mOsm). A suction electrode was used to deliver electrical stimuli to the attached dorsal roots at 0.1 Hz. The NMDAR-eEPSCs were recorded at the holding potential of +40 mV with the external solution containing bicuculline, strychnine, and CNQX. The input-output curves were plotted by eliciting the synaptic currents at five stimulation intensities (0.1, 0.2, 0.5, 1.0, and 2.0 mA). AMPAR-eEPSCs were recorded at the holding potential of −70 mV with bicuculline and strychnine added in the external solution. The monosynaptic responses were identified on the basis of the constant latency and absence of conduction failure in response to high-frequency electrical stimulation (20 Hz). AMPAR-mEPSCs and AMPAR-sEPSCs were recorded in the presence and absence of TTX (1 μM), respectively. The SOM^+ neurons expressing ChR2(H134R) were illuminated by blue light flashes (473 nm, 5 mW, 2 ms, 0.1 Hz), and the light-eEPSCs were recorded on the SPNs retrolabelled with CTB-488.

For current-clamp recordings, the glass pipettes had the resistance of 3 to 5 megohm when filled with the internal solution containing 135.0 mM K-gluconate, 3.0 mM KCl, 10.0 mM Hepes, 0.5 mM EGTA, 1.0 mM $MgCl_2$, 4.0 mM Mg-ATP, and 0.5 mM Na-GTP (pH 7.2 adjusted with KOH, 290 to 300 mOsm). The resting membrane potential was measured immediately after the establishment of whole-cell configuration. The membrane resistance was determined by hyperpolarizing current injections from −60 to 0 pA in 20-pA increments with the membrane potential held at −60 mV. The AP firings were elicited by injecting depolarizing currents in 2-pA increments from 0 to 40 pA at the holding potential of −60 mV. For spontaneous AP recordings, the neurons were held at the resting membrane potentials with no current injection. To record Aβ fiber-evoked AP firings, the spinal slices were perfused with normal ACSF. The dorsal roots were electrically stimulated at the intensity of 25 μA (*10*, *11*), and APs were recorded at resting membrane potentials.

HEK293T cells were transfected with pcDNA3.1 vector encoding GPR39 and GlyR α1 subunit. The pEGFP-N1 vector was co-transfected as the reporter plasmid. The cells were perfused (3 to 5 ml/min) at room temperature with bath solution containing 145.0 mM NaCl, 5.0 mM KCl, 2.0 mM $CaCl_2$, 1.0 mM $MgCl_2$, 10.0 Hepes, and 11.0 mM D-glucose (pH 7.3). The recording glass pipettes had the resistance of 3 to 5 megohm when filled with the internal solution [140.0 mM CsCl, 1.0 mM $CaCl_2$, 2.0 mM $MgCl_2$, 10.0 mM Hepes, 8.0 mM EGTA, 3.0 mM Na_2-ATP, and 0.1 mM Na-GTP (pH 7.2, 295 to 300 mOsm)]. The EGFP-positive cells were held at −80 mV, and the whole-cell currents were evoked by briefly puffing glycine (1 mM, 10 ms) onto the cells through an electrically controlled microperfusion system (MP2-S, InBio Inc., Wuhan, China) at an interval of 30 s. The series and input resistances were monitored online throughout each experiment. The recordings were discarded if the series or input resistance changed by more than 15%. The current signals were filtered at 2 kHz and sampled at 10 kHz.

Statistical analysis

All data were presented as means ± SEM and analyzed blindly. No statistical methods were used to predetermine sample sizes, which were chosen based on prior experience with similar experiments (*39*). Electrophysiological data were analyzed by Clampfit 8.0 or Mini-analysis software. The immunofluorescent images were analyzed by Image-Pro Plus 6.0 software. Western blot data were quantified by using NIH ImageJ software. Two group comparisons were conducted with paired Student's *t* test, Mann-Whitney *U* test, or Pearson's chi-square test. The data across multiple groups were compared by using Kruskal-Wallis test or one-way analysis of variance (ANOVA) followed by post hoc Bonferroni test. The data between multiple groups occurring over time were compared by using repeated measurement. The criterion for statistical significance was $P < 0.05$.

Supplementary Materials

This PDF file includes:

Figs. S1 to S15

REFERENCES AND NOTES

1. Y. Lu, H. Dong, Y. Gao, Y. Gong, Y. Ren, N. Gu, S. Zhou, N. Xia, Y. Y. Sun, R. R. Ji, L. Xiong, A feed-forward spinal cord glycinergic neural circuit gates mechanical allodynia. *J. Clin. Invest.* **123**, 4050–4062 (2013).
2. F. Moehring, P. Halder, R. P. Seal, C. L. Stucky, Uncovering the cells and circuits of touch in normal and pathological settings. *Neuron* **100**, 349–360 (2018).
3. C. Peirs, R. P. Seal, Neural circuits for pain: Recent advances and current views. *Science* **354**, 578–584 (2016).
4. J. Braz, C. Solorzano, X. Wang, A. I. Basbaum, Transmitting pain and itch messages: A contemporary view of the spinal cord circuits that generate gate control. *Neuron* **82**, 522–536 (2014).
5. R. Kuner, T. Kuner, Cellular circuits in the brain and their modulation in acute and chronic pain. *Physiol. Rev.* **101**, 213–258 (2021).
6. E. Foster, H. Wildner, L. Tudeau, S. Haueter, W. T. Ralvenius, M. Jegen, H. Johannssen, L. Hosli, K. Haenraets, A. Ghanem, K. K. Conzelmann, M. Bosl, H. U. Zeilhofer, Targeted ablation, silencing, and activation establish glycinergic dorsal horn neurons as key components of a spinal gate for pain and itch. *Neuron* **85**, 1289–1304 (2015).
7. C. A. Daniele, A. B. MacDermott, Low-threshold primary afferent drive onto GABAergic interneurons in the superficial dorsal horn of the mouse. *J. Neurosci.* **29**, 686–695 (2009).
8. C. Torsney, A. B. MacDermott, Disinhibition opens the gate to pathological pain signaling in superficial neurokinin 1 receptor-expressing neurons in rat spinal cord. *J. Neurosci.* **26**, 1833–1843 (2006).
9. A. J. Christensen, S. M. Iyer, A. Francois, S. Vyas, C. Ramakrishnan, S. Vesuna, K. Deisseroth, G. Scherrer, S. L. Delp, in vivo interrogation of spinal mechanosensory circuits. *Cell Rep.* **17**, 1699–1710 (2016).
10. B. Duan, L. Cheng, S. Bourane, O. Britz, C. Padilla, L. Garcia-Campmany, M. Krashes, W. Knowlton, T. Velasquez, X. Ren, S. Ross, B. B. Lowell, Y. Wang, M. Goulding, Q. Ma, Identification of spinal circuits transmitting and gating mechanical pain. *Cell* **159**, 1417–1432 (2014).
11. L. Cheng, B. Duan, T. Huang, Y. Zhang, Y. Chen, O. Britz, L. Garcia-Campmany, X. Ren, L. Vong, B. B. Lowell, M. Goulding, Y. Wang, Q. Ma, Identification of spinal circuits involved in touch-evoked dynamic mechanical pain. *Nat. Neurosci.* **20**, 804–814 (2017).
12. S. Choi, J. Hachisuka, M. A. Brett, A. R. Magee, Y. Omori, N. U. Iqbal, D. Zhang, M. M. DeLisle, R. L. Wolfson, L. Bai, C. Santiago, S. Gong, M. Goulding, N. Heintz, H. R. Koerber, S. E. Ross, D. D. Ginty, Parallel ascending spinal pathways for affective touch and pain. *Nature* **587**, 258–263 (2020).
13. T. Huang, S. H. Lin, N. M. Malewicz, Y. Zhang, Y. Zhang, M. Goulding, R. H. LaMotte, Q. Ma, Identifying the pathways required for coping behaviours associated with sustained pain. *Nature* **565**, 86–90 (2019).
14. M. C. Chiang, E. K. Nguyen, M. Canto-Bustos, A. E. Papale, A. M. Oswald, S. E. Ross, Divergent neural pathways emanating from the lateral parabrachial nucleus mediate distinct components of the pain response. *Neuron* **106**, 927–939.e5 (2020).
15. J. Deng, H. Zhou, J. K. Lin, Z. X. Shen, W. Z. Chen, L. H. Wang, Q. Li, D. Mu, Y. C. Wei, X. H. Xu, Y. G. Sun, The parabrachial nucleus directly channels spinal nociceptive signals to the intralaminar thalamic nuclei, but not the amygdala. *Neuron* **107**, 909–923.e6 (2020).
16. C. Nozaki, A. M. Vergnano, D. Filliol, A. M. Ouagazzal, A. Le Goff, S. Carvalho, D. Reiss, C. Gaveriaux-Ruff, J. Neyton, P. Paoletti, B. L. Kieffer, Zinc alleviates pain through high-affinity binding to the NMDA receptor NR2A subunit. *Nat. Neurosci.* **14**, 1017–1022 (2011).
17. J. Luo, A. Bavencoffe, P. Yang, J. Feng, S. Yin, A. Qian, W. Yu, S. Liu, X. Gong, T. Cai, E. T. Walters, C. W. Dessauer, H. Hu, Zinc Inhibits TRPV1 to Alleviate Chemotherapy-Induced Neuropathic Pain. *J. Neurosci.* **38**, 474–483 (2018).
18. C. Zhang, A. Dischler, K. Glover, Y. Qin, Neuronal signalling of zinc: From detection and modulation to function. *Open Biol.* **12**, 220188 (2022).
19. S. Kouvaros, M. Kumar, T. Tzounopoulos, Synaptic Zinc Enhances Inhibition Mediated by Somatostatin, but not Parvalbumin, Cells in Mouse Auditory Cortex. *Cereb. Cortex* **30**, 3895–3909 (2020).
20. C. T. Anderson, R. J. Radford, M. L. Zastrow, D. Y. Zhang, U. P. Apfel, S. J. Lippard, T. Tzounopoulos, Modulation of extrasynaptic NMDA receptors by synaptic and tonic zinc. *Proc. Natl. Acad. Sci. U.S.A.* **112**, E2705–E2714 (2015).
21. L. J. Blakemore, P. Q. Trombley, Zinc as a Neuromodulator in the Central Nervous System with a Focus on the Olfactory Bulb. *Front. Cell. Neurosci.* **11**, 297 (2017).
22. L. Marger, C. R. Schubert, D. Bertrand, Zinc: An underappreciated modulatory factor of brain function. *Biochem. Pharmacol.* **91**, 426–435 (2014).
23. A. Laitakari, L. Liu, T. M. Frimurer, B. Holst, The Zinc-Sensing Receptor GPR39 in Physiology and as a Pharmacological Target. *Int. J. Mol. Sci.* **22**, 3872 (2021).
24. S. Sato, X. P. Huang, W. K. Kroeze, B. L. Roth, Discovery and Characterization of Novel GPR39 Agonists Allosterically Modulated by Zinc. *Mol. Pharmacol.* **90**, 726–737 (2016).
25. P. Popovics, A. J. Stewart, GPR39: A Zn^{2+}-activated G protein-coupled receptor that regulates pancreatic, gastrointestinal and neuronal functions. *Cell. Mol. Life Sci.* **68**, 85–95 (2011).
26. M. Hershfinkel, The Zinc Sensing Receptor, ZnR/GPR39, in Health and Disease. *Int. J. Mol. Sci.* **19**, 439 (2018).
27. C. M. Davis, T. M. Bah, W. H. Zhang, J. W. Nelson, K. Golgotiu, X. Nie, F. N. Alkayed, J. M. Young, R. L. Woltjer, L. C. Silbert, M. R. Grafe, N. J. Alkayed, GPR39 localization in the aging human brain and correlation of expression and polymorphism with vascular cognitive impairment. *Alzheimers Dement.* **7**, e12214 (2021).
28. S. Xie, X. Jiang, D. M. Doycheva, H. Shi, P. Jin, L. Gao, R. Liu, J. Xiao, X. Hu, J. Tang, L. Zhang, J. H. Zhang, Activation of GPR39 with TC-G 1008 attenuates neuroinflammation via SIRT1/PGC-1α/Nrf2 pathway post-neonatal hypoxic-ischemic injury in rats. *J. Neuroinflammation* **18**, 226 (2021).
29. H. Luo, H. Z. Liu, W. W. Zhang, M. Matsuda, N. Lv, G. Chen, Z. Z. Xu, Y. Q. Zhang, Interleukin-17 Regulates Neuron-Glial Communications, Synaptic Transmission, and Neuropathic Pain after Chemotherapy. *Cell Rep.* **29**, 2384–2397.e5 (2019).
30. P. S. Miller, H. M. Da Silva, T. G. Smart, Molecular basis for zinc potentiation at strychnine-sensitive glycine receptors. *J. Biol. Chem.* **280**, 37877–37884 (2005).
31. Y. Zhang, A. Keramidas, J. W. Lynch, The Free Zinc Concentration in the Synaptic Cleft of Artificial Glycinergic Synapses Rises to At least 1 μM. *Front. Mol. Neurosci.* **9**, 88 (2016).
32. S. P. Meda Venkata, H. Li, L. Xu, J. Y. Koh, H. Nguyen, M. Minjares, C. Li, A. Kowluru, G. Milligan, J. M. Wang, Inhibition of GPR39 restores defects in endothelial cell-mediated neovascularization under the duress of chronic hyperglycemia: Evidence for regulatory roles of the sonic hedgehog signaling axis. *Proc. Natl. Acad. Sci. U.S.A.* **120**, e2208541120 (2023).
33. V. C. Cuzon Carlson, M. M. Ford, T. L. Carlson, A. Lomniczi, K. A. Grant, B. Ferguson, R. P. Cervera-Juanes, Modulation of Gpr39, a G-protein coupled receptor associated with alcohol use in non-human primates, curbs ethanol intake in mice. *Neuropsychopharmacology* **44**, 1103–1113 (2019).
34. G. Langlhofer, C. Villmann, The Intracellular Loop of the Glycine Receptor: It's not all about the Size. *Front. Mol. Neurosci.* **9**, 41 (2016).
35. R. J. Harvey, U. B. Depner, H. Wassle, S. Ahmadi, C. Heindl, H. Reinold, T. G. Smart, K. Harvey, B. Schutz, O. M. Abo-Salem, A. Zimmer, P. Poisbeau, H. Welzl, D. P. Wolfer, H. Betz, H. U. Zeilhofer, U. Muller, GlyR alpha3: An essential target for spinal PGE2-mediated inflammatory pain sensitization. *Science* **304**, 884–887 (2004).
36. I. Del Pino, D. Koch, R. Schemm, B. Qualmann, H. Betz, I. Paarmann, Proteomic analysis of glycine receptor β subunit (GlyRβ)-interacting proteins: Evidence for syndapin I regulating synaptic glycine receptors. *J. Biol. Chem.* **289**, 11396–11409 (2014).
37. I. del Pino, I. Paarmann, M. Karas, M. W. Kilimann, H. Betz, The trafficking proteins Vacuolar Protein Sorting 35 and Neurobeachin interact with the glycine receptor β-subunit. *Biochem. Biophys. Res. Commun.* **412**, 435–440 (2011).
38. C. G. Specht, N. Grunewald, O. Pascual, N. Rostgaard, G. Schwarz, A. Triller, Regulation of glycine receptor diffusion properties and gephyrin interactions by protein kinase C. *EMBO J.* **30**, 3842–3853 (2011).
39. Z. Y. Zhang, H. H. Bai, Z. Guo, H. L. Li, Y. T. He, X. L. Duan, Z. W. Suo, X. Yang, Y. X. He, X. D. Hu, mGluR5/ERK signaling regulated the phosphorylation and function of glycine receptor α1ins subunit in spinal dorsal horn of mice. *PLoS Biol.* **17**, e3000371 (2019).
40. L. Besser, E. Chorin, I. Sekler, W. F. Silverman, S. Atkin, J. T. Russell, M. Hershfinkel, Synaptically released zinc triggers metabotropic signaling via a zinc-sensing receptor in the hippocampus. *J. Neurosci.* **29**, 2890–2901 (2009).
41. J. W. Lynch, Molecular structure and function of the glycine receptor chloride channel. *Physiol. Rev.* **84**, 1051–1095 (2004).
42. L. Li, L. Shi, Y. M. Xu, X. Yang, Z. W. Suo, X. D. Hu, GABAergic inhibition regulated pain sensitization through STEP61 signaling in spinal dorsal horn of mice. *Anesthesiology* **122**, 686–697 (2015).
43. H. Y. Peng, G. D. Chen, C. Y. Lai, M. C. Hsieh, T. B. Lin, Spinal SIRPα1-SHP2 interaction regulates spinal nerve ligation-induced neuropathic pain via PSD-95-dependent NR2B activation in rats. *Pain* **153**, 1042–1053 (2012).
44. B. Holst, K. L. Egerod, E. Schild, S. P. Vickers, S. Cheetham, L. O. Gerlach, L. Storjohann, C. E. Stidsen, R. Jones, A. G. Beck-Sickinger, T. W. Schwartz, GPR39 signaling is stimulated by zinc ions but not by obestatin. *Endocrinology* **148**, 13–20 (2007).
45. C. Hanack, M. Moroni, W. C. Lima, H. Wende, M. Kirchner, L. Adelfinger, K. Schrenk-Siemens, A. Tappe-Theodor, C. Wetzel, P. H. Kuich, M. Gassmann, D. Roggenkamp, B. Bettler, G. R. Lewin, M. Selbach, J. Siemens, GABA blocks pathological but not acute TRPV1 pain signals. *Cell* **160**, 759–770 (2015).
46. M. Tena-Campos, E. Ramon, D. O. Borroto-Escuela, K. Fuxe, P. Garriga, The zinc binding receptor GPR39 interacts with 5-HT1A and GalR1 to form dynamic heteroreceptor complexes with signaling diversity. *Biochim. Biophys. Acta* **1852**, 2585–2592 (2015).
47. W. Wang, Y. Qiao, Z. Li, New Insights into Modes of GPCR Activation. *Trends Pharmacol. Sci.* **39**, 367–386 (2018).

48. K. Mlyniec, D. Siodlak, U. Doboszewska, G. Nowak, GPCR oligomerization as a target for antidepressants: Focus on GPR39. *Pharmacol. Ther.* **225**, 107842 (2021).
49. B. Laube, J. Kuhse, N. Rundstrom, J. Kirsch, V. Schmieden, H. Betz, Modulation by zinc ions of native rat and recombinant human inhibitory glycine receptors. *J. Physiol.* **483**, 613–619 (1995).
50. L. Storjohann, B. Holst, T. W. Schwartz, Molecular mechanism of Zn^{2+} agonism in the extracellular domain of GPR39. *FEBS Lett.* **582**, 2583–2588 (2008).
51. L. Li, M. Rutlin, V. E. Abraira, C. Cassidy, L. Kus, S. Gong, M. P. Jankowski, W. Luo, N. Heintz, H. R. Koerber, C. J. Woodbury, D. D. Ginty, The functional organization of cutaneous low-threshold mechanosensory neurons. *Cell* **147**, 1615–1627 (2011).
52. Y. Z. Li, Y. B. Zhu, A. N. Ge, M. Gao, K. L. Wang, X. R. Zeng, J. Li, Y. Li, J. Y. Xu, H. H. Bai, S. J. Wu, Reduced expression of APLP2 in spinal GABAergic inhibitory neurons contributed to nerve injury-induced microglial activation and pain sensitization. *Neuropharmacology* **224**, 109334 (2023).
53. G. Corder, B. Ahanonu, B. F. Grewe, D. Wang, M. J. Schnitzer, G. Scherrer, An amygdalar neural ensemble that encodes the unpleasantness of pain. *Science* **363**, 276–281 (2019).
54. Z. Y. Zhang, H. H. Bai, Z. Guo, H. L. Li, X. T. Diao, T. Y. Zhang, L. Yao, J. J. Ma, Z. Cao, Y. X. Li, X. Bai, H. K. Chen, Z. W. Suo, X. Yang, X. D. Hu, Ubiquitination and functional modification of GluN2B subunit-containing NMDA receptors by Cbl-b in the spinal cord dorsal horn. *Sci. Signal.* **13**, eaaw1519 (2020).
55. H. Petitjean, F. B. Bourojeni, D. Tsao, A. Davidova, S. G. Sotocinal, J. S. Mogil, A. Kania, R. Sharif-Naeini, Recruitment of Spinoparabrachial Neurons by Dorsal Horn Calretinin Neurons. *Cell Rep.* **28**, 1429–1438.e4 (2019).
56. T. King, L. Vera-Portocarrero, T. Gutierrez, T. W. Vanderah, G. Dussor, J. Lai, H. L. Fields, F. Porreca, Unmasking the tonic-aversive state in neuropathic pain. *Nat. Neurosci.* **12**, 1364–1366 (2009).
57. A. Andrianarivelo, E. Saint-Jour, P. Pousinha, S. P. Fernandez, A. Petitbon, V. De Smedt-Peyrusse, N. Heck, V. Ortiz, M. C. Allichon, V. Kappes, S. Betuing, R. Walle, Y. Zhu, C. Josephine, A. P. Bemelmans, G. Turecki, N. Mechawar, J. A. Javitch, J. Caboche, P. Trifilieff, J. Barik, P. Vanhoutte, Disrupting D1-NMDA or D2-NMDA receptor heteromerization prevents cocaine's rewarding effects but preserves natural reward processing. *Sci. Adv.* **7**, eabg5970 (2021).
58. T. E. Tracy, J. Madero-Perez, D. L. Swaney, T. S. Chang, M. Moritz, C. Konrad, M. E. Ward, E. Stevenson, R. Huttenhain, G. Kauwe, M. Mercedes, L. Sweetland-Martin, X. Chen, S. A. Mok, M. Y. Wong, M. Telpoukhovskaia, S. W. Min, C. Wang, P. D. Sohn, J. Martin, Y. Zhou, W. Luo, J. Q. Trojanowski, V. M. Y. Lee, S. Gong, G. Manfredi, G. Coppola, N. J. Krogan, D. H. Geschwind, L. Gan, Tau interactome maps synaptic and mitochondrial processes associated with neurodegeneration. *Cell* **185**, 712–728.e14 (2022).
59. Y. Riku, Y. Iwasaki, S. Ishigaki, A. Akagi, M. Hasegawa, K. Nishioka, Y. Li, M. Riku, T. Ikeuchi, Y. Fujioka, H. Miyahara, J. Sone, N. Hattori, M. Yoshida, M. Katsuno, G. Sobue, Motor neuron TDP-43 proteinopathy in progressive supranuclear palsy and corticobasal degeneration. *Brain* **145**, 2769–2784 (2022).
60. V. Fernandez-Duenas, J. Bonaventura, E. Aso, R. Lujan, S. Ferre, F. Ciruela, Overcoming the Challenges of Detecting GPCR Oligomerization in the Brain. *Curr. Neuropharmacol.* **20**, 1035–1045 (2022).

Acknowledgments: We thank the NHC Key Laboratory of Diagnosis and Therapy of Gastrointestinal Tumor of Gansu Provincial Hospital for providing confocal laser scanning microscope. **Funding:** This work was supported by the National Natural Science Foundation of China grants 81973296 (to X.-D.H.), 32170997 (to X.-D.H.), and 82073822 (to Z.-W.S.) and School of Pharmacy and State Key Laboratory of Applied Organic Chemistry, Lanzhou University, P.R. China. **Author contributions:** Immunohistochemistry, recordings, and PLA: H.-H.B. Behavioral tests: K.-L.W., X.-R.Z., J.L., Y.L., J.-Y.X., and Y.Z., Immunoprecipitation, GST pull-down assay, and Western blot: H.-F.J., X.Y., and Z.-W.S. Data analysis: X.-D.H. and H.-H.B. Conceptualization and experimental design: X.-D.H. Writing—original draft as well as review and editing: X.-D.H. **Competing interests:** The authors declare that they have no competing interests. **Data and materials availability:** All data needed to evaluate the conclusions in the paper are present in the paper and/or the Supplementary Materials.

Submitted 5 July 2023
Accepted 4 January 2024
Published 2 February 2024
10.1126/sciadv.adj3808